Earth Syst. Sci. Data, 15, 1329–1355, 2023
https://doi.org/10.5194/essd-15-1329-2023

Open Access Earth System Science Data

Lake surface temperature retrieved from Landsat satellite series (1984 to 2021) for the North Slave Region

Gifty Attiah[1,2], Homa Kheyrollah Pour[1,2], and K. Andrea Scott[3]

[1]Remote Sensing of Environmental Change (ReSEC) Research group, Department of Geography and Environmental Studies, Wilfrid Laurier University, 75 University Avenue West, Waterloo N2L 3C5, Canada
[2]Cold Regions Research Centre, Wilfrid Laurier University, Waterloo, ON, Canada
[3]Department of Systems Design Engineering, University of Waterloo, 200 University Avenue, West, Waterloo N2L 3G1, Canada

Correspondence: Gifty Attiah (gattiah@wlu.ca)

Received: 18 August 2022 – Discussion started: 10 October 2022
Revised: 10 February 2023 – Accepted: 13 February 2023 – Published: 23 March 2023

Abstract. Lake surface temperature (LST) is an important attribute that highlights regional weather and climate variability and trends. The spatial resolution and thermal sensors on Landsat platforms provide the capability of monitoring the temporal and spatial distribution of lake surface temperature on small- to medium-sized lakes. In this study, a retrieval algorithm was applied to the thermal bands of Landsat archives to generate a LST dataset (North Slave LST dataset) for 535 lakes in the North Slave Region (NSR) of the Northwest Territories (NWT), Canada, for the period of 1984 to 2021. North Slave LST was retrieved from Landsat 5 Thematic Mapper (TM), Landsat 7 Enhanced Thematic Mapper Plus (ETM+), and Landsat 8 Operational Land Imager (OLI) and the Thermal Infrared Sensor (TIRS); however, most of the dataset was created from the thermal bands of Landsat 5 (43 %) due to its longevity (1984–2013). Cloud masks were applied to Landsat images to eliminate cloud cover. In addition, a 100 m inward buffer was applied to lakes to prevent pixel mixing with shorelines. To evaluate the algorithm applied, retrieved LST was compared with in situ data and Moderate Resolution Imaging Spectroradiometer (MODIS) LST observations. A good agreement was observed between in situ observations and North Slave LST, with a mean bias of 0.12 °C and a root mean squared deviation (RMSD) of 1.7 °C. The North Slave LST dataset contains more available data for warmer months (May to September; 57.3 %) compared to colder months (October to April). The average number of images per year for each lake across the NSR ranged from 20 to 45. The North Slave LST dataset, available at https://doi.org/10.5683/SP3/J4GMC2 (Attiah et al., 2022), will provide communities, scientists, and stakeholders with spatial and temporal changing temperature trends on lakes for the past 38 years.

1 Introduction

Lake surface temperature (LST) is a significant indicator of climate change and is crucial to lake ecosystems (Livingstone et al., 2005; Zhang et al., 2019). Several ecological, biological, and hydrogeochemical processes are influenced by temperature in lakes (Schneider and Hook, 2010). Lake warming can result in a decrease in ice cover, changes in over-lake wind speeds, and changes in water column stratification (Austin and Colman, 2007; Desai et al., 2009; Kraemer et al., 2015; Magnuson et al., 2000). The land–water–atmosphere system's energy and material exchange processes can also be reflected in lake surface temperature (Huang et al., 2017; Yang et al., 2020) and is hence recognised as an essential climate variable. As a significant variable in regional studies, the impact and relationship of LST to weather, climate, and lake processes have been explored by other studies, including influences on the weather (Eerola et al., 2014; Kheyrollah Pour et al., 2017, 2014a, b), climate (Moigne et al., 2016; Wang et al., 2022), precipitation

(Zhang et al., 2016), lake effect snow (Shi and Xie, 2019), and lake overturning (Fichot et al., 2019). Observations of lakes worldwide have reported increased lake temperatures associated with global warming, resulting in changes to the underlying lake system (O'Reilly et al., 2015; Woolway et al., 2019). Long-term records of lake surface temperature are therefore necessary to understand the thermal mechanism underlying lake processes, including lake ice formation and decay, lake productivity, aquatic ecosystems, and other limnological processes (Chen et al., 2019; Collingsworth et al., 2017; Woolway et al., 2020).

Even though in situ records on lake surface temperature are a good source of temperature data for lake studies, their sparse distribution, especially in the north, presents a challenge, making satellite-derived data an essential resource in regional and global studies. Satellite sensors like MODIS (Moderate Resolution Imaging Spectroradiometer) and AVHRR (Advanced Very High-Resolution Radiometer) have been heavily relied upon to estimate and analyse LST in several studies (e.g. Kheyrollah Pour et al., 2014b; Wloczyk et al., 2006; Sima et al., 2013; Wan et al., 2002; Zhao et al., 2020; Reinart and Reinhold, 2008); however, their application to small and medium lakes is limited due to their relatively moderate spatial resolution ($\sim$ 250 m–1 km). In addition, satellite-retrieved LST datasets for global studies like the Global Lake Temperature Collaboration (GLTC) have a low sampling of high-latitude lakes, restricting their use for climate studies in these northern regions. Satellites like Landsat, however, provide an opportunity for regional studies of lake processes, including the spatial extraction of LST on Arctic and Subarctic lakes. The strength of Landsat includes its high spatial resolution (30–120 m), high radiometric resolution (8–12 bit), and the presence of thermal infrared bands for the retrieval of LST. In addition, the longevity of data archives makes it one of the vastest and most extended observations of Earth's surface water from space (Pekel et al., 2016). Currently, a regional spatial lake surface temperature dataset for small- and medium-sized lakes on a large scale does not exist in the Northwest Territories (NWT) in Canada, specifically for North Slave Region (NSR) lakes. This study aims to bridge this gap by utilising Landsat's capabilities.

In this study, we generated LST data (North Slave LST) for over 535 predominantly small to medium lakes using data obtained from Landsat archives (Landsat 5 TM, Landsat 7 ETM+, and Landsat 8 OLI/TIRS). An adapted temperature retrieval algorithm (Jimenez-Munoz et al., 2009, 2014) is applied to the thermal bands of Landsat to estimate LST. The dataset produced has a spatial resolution of 30 m and varying temporal resolution due to differences in satellite overpass and cloud interference. The generated North Slave LST dataset was evaluated with in situ datasets and compared with the widely used LST satellite data (MODIS). The temporal and spatial distribution of the dataset is presented to report on data availability patterns. Additionally, the North Slave LST dataset is used to briefly highlight the spatial inter-lake and intra-lake distribution of LST on NSR lakes.

This study aims to (i) capitalise on the thermal bands of Landsat to create an up-to-date lake surface temperature dataset for the NSR to record distribution from 1984 to 2021, (ii) highlight the temporal and spatial heterogeneity of LST between and within lakes on a 30 m grid, and (iii) distribute and publish LST data for stakeholders, research communities, to enable further research, the public, and the Government of the Northwest Territories to facilitate decision-making processes.

2 Study lakes and data sources

2.1 Selected lakes in North Slave Region, NWT

The North Slave LST data are generated for 535 lakes between latitude 61 and 67° N and longitude −120 and −102° W of the Northwest Territories (NWT) located in northern Canada, covering an area of about 316 000 km^2 (Fig. 1a). The region lies in the Slave Province of the Canadian Shield and is interspersed with numerous lakes (>10 000) of various sizes. The average elevation in the NSR is 301 m, with the lake elevation ranging from 138 to 624 m (Messager et al., 2016). This dataset contains LST on lakes with surface areas ranging from 0.05 to 1680 km^2, mean depths ranging from 1 to 63 m, and volumes ranging from 0.24 to 27 321 km^3. Appendix A contains a table listing all the study lakes and their geophysical properties. Air temperature in the NSR ranges from $\sim$ −45 to +30 °C. Most study lakes are between 1 and 5 km^2 (Fig. 1b), and the dominant mean depth range is from 5 to 10 m (Fig. 1c).

2.2 Spatial data for LST retrieval

2.2.1 Landsat archives

Landsat archives consist of optical data from a series of Earth-observing satellite missions. For this study, Landsat tiles covering the NSR were obtained from the United States Geological Survey (USGS). Surface temperatures on lakes were estimated from the thermal infrared (TIR) bands of Landsat 5 TM (Thematic Mapper; 1984–2013), Landsat 7 ETM+ (Enhanced Thematic Mapper Plus; 1999–present), and Landsat 8 OLI/TIRS (Operational Land Imager and the Thermal Infrared Sensor; 2013–present) instruments. Landsat instruments orbit at an altitude of 705 km, are sun-synchronous, and have a 16 d repeat cycle. The thermal band (band 6) of Landsat 5 and Landsat 7 record emitted radiation between the wavelengths of 10.40 and 12.50 µm, while that of Landsat 8 (band 10) records between 10.6 and 11.19 µm. The spatial resolution of the thermal bands for Landsat 5 TM (120 m), Landsat 7 ETM+ (60 m), and Landsat 8 OLI/TIRS (100 m) are resampled with the cubic convolution method and distributed at a spatial resolution of 30 m to match optical bands (USGS, 2022). In addition, other bands, includ-

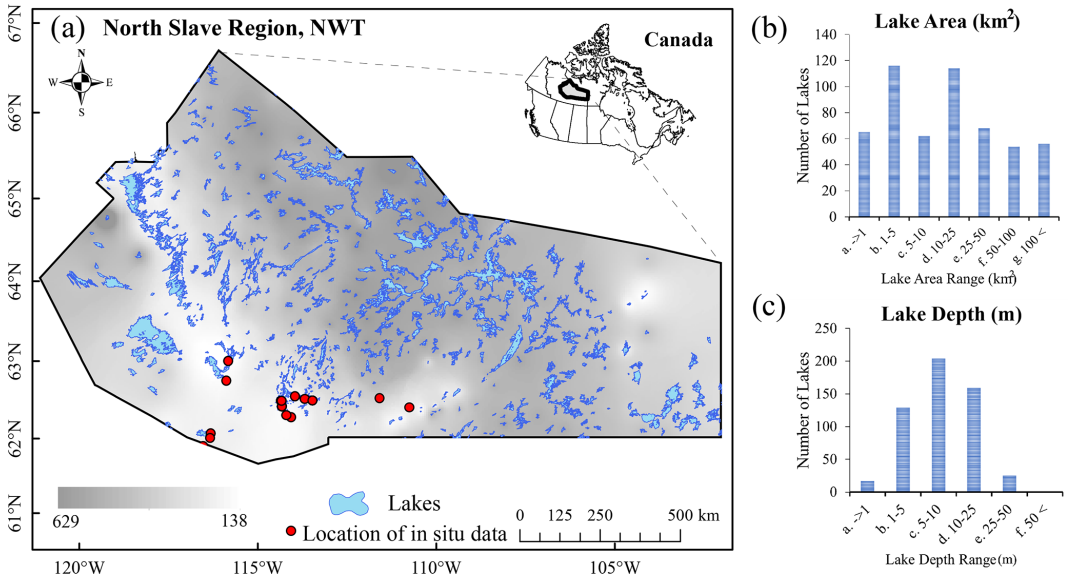

Figure 1. **(a)** Geographic distribution of study lakes in the North Slave Region, Northwest Territories, Canada. The lake area and depth distribution are shown in panels **(b)** and **(c)**, respectively.

ing the quality band (BQA), near-infrared band, red band, and metadata, are also used in the retrieval of LST. About 34 Landsat tile scenes cover the NSR, with each tile containing 5000 × 5000 30 m pixels and overpass times ranging from 18:00 to 20:00 UTC.

2.2.2 ERA5 reanalysis data

Total column water vapour obtained from ERA5 reanalysis data (Copernicus Climate Change Service – C3S) from 1984 to 2021 was used as input in the algorithm to correct for atmospheric effects on Landsat images. Values were derived from the hourly data, with a ∼ 30 km spatial resolution obtained from the European Centre for Medium-Range Weather Forecasts (ECMWF; Hersbach et al., 2020). ERA5 reanalysis data are a dataset generated from a combination of in situ observations and modelling to provide estimates of land, atmospheric, and ocean changes on a global scale. Average ERA5 hourly total column water vapour on single levels was used as an input in the LST retrieval algorithm.

2.2.3 Lake outline and properties data

Each lake's name, location, depth, size, elevation, and outline were retrieved from a combination of the HydroLAKES database, CanVec Series, and the Water File – Lakes and Rivers database. The HydroLAKES database is a digital map repository developed in the Global HydroLAB (http://wp.geog.mcgill.ca/hydrolab/, last access: 20 May 2022) from a collection of several databases (e.g. global and regional databases like CanVec Series and Shuttle Radar Topography Mission, SRTM, Water Body Data; Slater et al., 2006). This database provides information on world lakes and their significant properties through high-resolution maps. Over 1 427 688 individual lake vector polygons greater than 10 ha are included in the repository (Messager et al., 2016). The mode of pixel-level lake elevation data obtained from the EarthEnv-DEM90 (digital elevation model) and the USGS-provided GTOPO30 DEM was used to calculate the HydroLAKES elevation data. A geostatistical model developed from surrounding land surface topography was derived to generate average lake depths and volumes (Messager et al., 2016). As part of the Government of Canada initiative (https://open.canada.ca, last access: 28 March 2022), the CanVec Series provides a geometric description and fundamental characteristics of hydrographic phenomena in the form of geospatial vector data. The Water File – Lakes and Rivers (polygons) data (https://www12.statcan.gc.ca, last access: 30 March 2022) maps lakes and rivers under the 2006 census, as created by Statistics Canada under the Government of Canada on 29 August 2013. These data were the primary source of lake names attributed to lake outlines in our dataset.

2.2.4 Evaluation dataset

Landsat-derived LST was generated during both open-water and ice-covered seasons. Retrieved data were evaluated against in situ measurements collected over selected locations within the study area (Fig. 1). In situ measurements from Mackenzie DataStream were used for evaluating LST derived from Landsat. DataStream is an open-access freshwater data platform that provides water-monitoring data collected by governments and communities across Canada. The database for the NWT region was the product of the NWT-

wide community-based water quality monitoring (CBM) programme, which is collected during open-water seasons. The CBM programme was implemented in 2012 as part of a partnership between the Department of Environment and Natural Resources (ENR), the Government of the Northwest Territories (GNWT), communities, and regional organisations in NWT to monitor water quality and changes. The surface temperatures on lakes were measured with YSI sondes and EXO2 sondes and interpreted by ENR. Collated surface temperature data used for evaluation from this source were from the years 2014 to 2019. Another primary source was lake temperature data collected by Environment and Climate Change Canada (ECCC) from 1999 to 2003. Temperature loggers were used to measure hourly temperature on lakes during open water periods; however, only temperature collected at the skin surface (depth = 0 m) was used for LST evaluation in this study.

The MODIS (MYD11_L2) surface temperature dataset from 2003 to 2021 was used to evaluate the Landsat-derived LST data generated during both open-water and ice-covered seasons. The dataset was obtained from NASA's Earth Observing System Data and Information System (EOSDIS), mounted on the Terra and Aqua satellites; MODIS records within the spectral ranges of 0.405–14.385 µm across 36 bands. The Aqua product contains nighttime and daytime LST measurements on a spatial resolution of ∼ 1 km derived from the thermal infrared bands. For this study, the daytime LST measurement covering lakes in the NSR was compared against the Landsat-derived LST.

3 Methods

3.1 Algorithm for lake surface temperature

The thermal bands of Landsat were used in the retrieval algorithm to generate North Slave LST (band 6 for Landsat 5TM/Landsat 7ETM+ and band 10 for Landsat OLI/TIRS). Atmospheric and emissivity correction of thermal bands were conducted to account for the effect of absorption and emission of surface radiation. A single channel (SC) method was adapted and applied in this study to retrieve LST (Jimenez-Munoz et al., 2009, 2014; Jiménez-Muñoz and Sobrino, 2003). This method is based on approximating the radiative transfer equation without the dependence on in situ radio-sounding data. Only a single band is required in the SC method, making it feasible for use on single thermal band satellites like Landsat 5 TM, which was utilised in this study. The SC method uses atmospheric water vapour (Sect. 2.2.2) as a variable in the correction for atmospheric effect.

LST retrieval using the SC method requires atmospheric water vapour, emissivity, brightness-temperature- and wavelength-emitted radiance values, and thermal constants. The LST estimation is based on the following (Jiménez-Munoz and Sobrino, 2003):

$$\mathrm{LST} = \gamma\left[\varepsilon^{-1}\left(\psi_1 L_{\mathrm{sensor},\lambda} + \psi_2\right) + \psi_3\right] + \delta, \tag{1}$$

where

$$\gamma = \left\{\frac{c_2 L_{\mathrm{sensor},\lambda}}{T^2_{\mathrm{sensor}}}\left[\frac{\lambda^4}{c_1}L_{\mathrm{sensor},\lambda} + \lambda^{-1}\right]\right\}^{-1}, \tag{2}$$

and

$$\delta = -\gamma L_{\mathrm{sensor},\lambda} + T_{\mathrm{sensor}}. \tag{3}$$

At-sensor radiance and brightness temperature are denoted by $L_{\mathrm{sensor},\lambda}$ (W m^{-2} sr^{-1} µm^{-1}) and T_{sensor} (K), respectively. c_1 (1.19104 10^8 W µm^4 m^{-2} sr^{-1}) and c_2 (14387.7 µm K) are Planck's constants. The emitted radiance wavelength (λ) is 11.457 µm in Landsat 5 TM, 11.269 µm in Landsat 7 ETM+, and 10.904 µm in Landsat 8 OLI TIRS. ψ_1, ψ_2 and ψ_3 are atmospheric functions obtained as a function of water vapour (w) and are specific to the three individual Landsat sensors.

At-sensor spectral radiance was calculated from raw digital numbers (DNs) of thermal bands based on metadata information and constants. Equations used are specific to the type of sensor, as listed below.

At-sensor radiance values for Landsat 5 TM were derived using Eq. (4) as follows (Chander and Markham, 2003):

$$L_{\mathrm{sensor},\lambda} = G_{\mathrm{rescale}} \cdot Q_{\mathrm{cal}} + B_{\mathrm{rescale}}, \tag{4}$$

where 0.0551584 Wm^2 sr^1 µm^1/DN and 1.2378 Wm^2 sr^1 µm^1/DN are constants for G_{rescale} and B_{rescale}, respectively.

Landsat 7 ETM+'s at-sensor radiance values were derived using Eq. (5) as follows (Ihlen and Zanter, 2019):

$$L_{\mathrm{sensor},\lambda} = \left(\frac{L_{\lambda\mathrm{max}} - L_{\lambda\mathrm{min}}}{Q_{\mathrm{calmax}} - Q_{\mathrm{calmin}}}\right)(Q_{\mathrm{cal}} - Q_{\mathrm{calmin}}) + L_{\lambda\mathrm{min}}, \tag{5}$$

where the maximum and minimum spectral radiance is represented by $L_{\lambda\mathrm{max}}$ and $L_{\lambda\mathrm{min}}$, respectively, and the maximum and minimum quantised calibrate pixel is represented by Q_{calmax} and Q_{calmin}, respectively, as obtained from the metafile. Q_{cal} denotes DN values of pixels in band 6.

Landsat 8 OLI TIRS's at-sensor radiance values were derived using Eq. (6) as follows (U.S. Geological Survey, 2016):

$$L_{\mathrm{sensor},\lambda} = M_L Q_{\mathrm{cal}} + A_L, \tag{6}$$

where the DN values of pixels in band 10 are denoted by Q_{cal}. $M_L = 0.000342$ and $A_L = 0.1$ are fixed rescaling factors in the metadata provided by the USGS.

Brightness temperature T_{sensor} is estimated using calculated at-sensor radiance values and thermal constants derived from the metadata based on Eq. (7) below:

$$T_{\mathrm{sensor}} = \frac{K_2}{\ln\left(\frac{K_1}{L_{\mathrm{sensor},\lambda}} + 1\right)}, \tag{7}$$

Table 1. Thermal constants applied to Landsat thermal bands for brightness temperature estimation.

Thermal Constant	Landsat 5 TM Band 6	Landsat 7 ETM+ Band 6	Landsat 8 OLI/TIRS Band 10
K_1	607.76	666.09	774.8853
K_2	1260.56	1282.71	1321.0789

where thermal constants K_1 ($\mathrm{W\,m^{-2}\,sr^{-1}\,\mu m^{-1}}$) and K_2 (K) vary based on the type of Landsat sensor (Table 1).

The atmospheric functions (AFs) used for atmospheric correction were based on coefficients acquired using Global Atmospheric Profiles derived from Reanalysis Information (GAPRI) and Thermodynamic Initial Guess Retrieval (TIGR) databases (Jimenez-Munoz et al., 2009, 2014).

Atmospheric function equations ψ_1, ψ_2 and ψ_3, particularised for Landsat 8 OLI/TIRS, are as follows:

$$\psi_1 = 0.04019w^2 + 0.02916w + 1.01523, \quad (8a)$$

$$\psi_2 = -0.38333w^2 - 0.50294w + 0.20324, \quad (8b)$$

$$\psi_1 = 0.00918w^2 + 1.36072w - 0.27514. \quad (8c)$$

Landsat 7 ETM+'s AFs are as follows:

$$\psi_1 = 0.07593w^2 - 0.07132w + 1.08565, \quad (9a)$$

$$\psi_1 = -0.61438w^2 - 0.70916w - 0.19379, \quad (9b)$$

$$\psi_1 = -0.02892w^2 + 1.46051w - 43\,199. \quad (9c)$$

Landsat 5 TM's AFs are as follows:

$$\psi_1 = 0.07518w^2 - 0.00492w + 1.03189, \quad (10a)$$

$$\psi_1 = -0.59600w^2 - 1.22554w + 0.08104, \quad (10b)$$

$$\psi_1 = -0.02767w^2 + 1.43740w - 0.25844. \quad (10c)$$

The normalised difference vegetation index (NDVI; Eq. 11) values calculated were used to assign lake surface emissivity. Near-infrared (NIR) and red bands of Landsat were used to calculate NDVI values (Eq. 11).

$$\mathrm{NDVI} = \frac{\mathrm{NIR} - \mathrm{Red}}{\mathrm{NIR} + \mathrm{Red}} \quad (11)$$

The lake surface was assigned an emissivity of 0.985 if the NDVI values were lower than 0.05; otherwise, a value of 0.97 was assigned (Prats et al., 2018).

3.2 Retrieval of lake surface temperature

3.2.1 LST retrieval

LST retrieval algorithms were applied to the thermal bands in conjunction with other processed output (bands and metadata) from Landsat data to generate the North Slave LST dataset. A quality assurance (QA) band, outlining the surface, atmosphere, and sensor conditions included in the Landsat data, was used to mask clouds and other obstructions. The QA band assesses cloud influence at different confidence levels (high, with 67 %–100 %, medium, with 34 %–66 %, and low, with 0 %–33 %), making it possible for cloud removal. This study categorised high and medium confidence values as cloud pixels, while low confidence values were considered to be cloud-free. LST retrieval algorithms and equations (Eqs. 1–11) were applied to the thermal bands of all tiles from 1984 to 2021. Cloud masks were generated and applied to retrieved LST to eliminate cloud-distorted pixels. LST pixels were extracted using the vector files of lake outlines from the HydroLAKES dataset. A 100 m negative buffer was applied to remove the effect of lake pixel mixing with land surface pixels. Possible erroneous pixels were flagged using z scores which calculate how far a value is from the mean. This was used to access spatial differences and outliers in pixels. Pixels of lakes with z-score values above 3.5 and below -3.5 were flagged. In addition, LST output with equal pixels across the entire lake or group of pixels having the same value to four decimal places were flagged. Further visual quality checks and analysis were applied to flagged LST to clean the generated data and remove the erroneous cloud cover that the masks could not capture. The overall framework for the retrieval and generation of the LST dataset for selected lakes in the NSR is highlighted in Fig. 2.

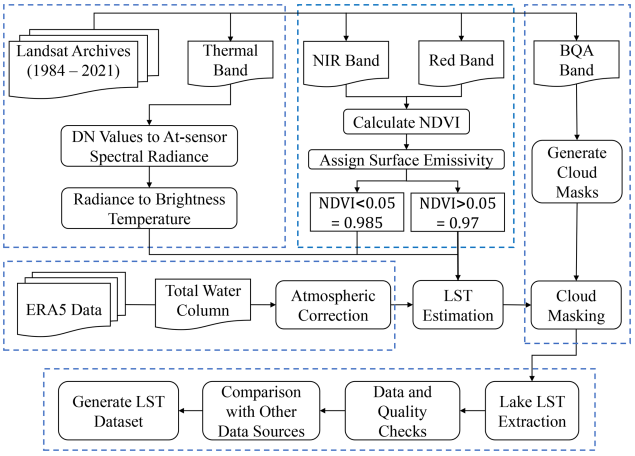

Figure 2. Workflow and methods for generating North Slave LST dataset from Landsat archives.

3.2.2 Data quality assessment information

It is essential to highlight the limitations of data estimates from satellite-based records (Merchant et al., 2017). This provides an awareness of the degree to which a sensor is stable, in addition to the observations obtained from them. Additionally, these reports are necessary to inform the confidence of the data extracted and the structures of their errors through time and space. One significant distortion of the Landsat archives is the failure of the scan line corrector (SLC) of Landsat 7 ETM+ on 31 May 2003. As a result, the measurement from scans could not be corrected, causing all images sensed after that date to lose about 22 % of the data extracted. This limitation, named Landsat 7 ETM+ SLC-off issue, is more prominent at the edges of images than in the centre. Nevertheless, Landsat 7 ETM+ data were still used in the study because the radiometric and geometric corrections are unaffected by this scan line issue.

3.2.3 Evaluation methods

Indicators used to evaluate the performance of North Slave LST against in situ and MODIS LST were the root mean squared deviation (RMSD), mean bias deviation (MBD), and R squared (R^2). The MBD assesses systematic differences and evaluates the underprediction and overprediction between two datasets (Eq. 12). A MBD value of 0 indicates an utterly random error.

$$\mathrm{MBD} = \frac{\sum_{i=1}^{N}[P_i - O_i]}{N}, \tag{12}$$

where O_i and P_i are the observed and generated values, respectively, while N is the number of points used for evaluation. The index values ranged between 0 and 1, indicating the worst and best possible performance.

The root mean squared deviation (RMSD) measures the total difference between the two datasets without distinguishing between the over- or underprediction of models and/or algorithms (Eq. 13). No deviation in the values results in a RMSD value of 0.

$$\mathrm{RMSD} = \sqrt{\frac{\sum_{i=1}^{N}[P_i - O_i]^2}{N}} \tag{13}$$

4 Results and discussion

4.1 Quality of North Slave LST

The primary sources of limitation for the North Slave LST data include (i) potential mixed pixels that might not be captured by the algorithm, (ii) the presence of "no data" pixels on lakes, and (iii) inconsistency in the temporal resolution of dataset per lake. The lake boundaries' extraction of LST was based on outlines from external boundary files (Sect. 2.2.4). As such, errors that may exist, including overestimating lake area and the inability to accurately demarcate lake islands, would affect the LST values retrieved. A 100 m inward buffer was applied to address this; however, valuable lake shore LST information is lost, especially in small lakes. The number of pixels and the percentage of the lake it represents is reported in Appendix A. Depending on the lake shape, area, and existence of islands, the pixels represented 16.7 % to 97.34 % of the lake area. The spatial variation in LST is reduced for lakes with a smaller number of pixels.

In addition to the overall representativeness of pixels on lakes, LST pixels retrieved for a given day may vary due to cloud cover and the Landsat 7 ETM+ SLC-off issue (Sect. 3.2.2), resulting in missing LST pixels for a given lake. The dataset represents these missing LST pixels with no data pixels (which do not contain LST values). Figure 3 highlights the fraction of LST pixels to no data pixels distributed over years and months. The percentage of no data pixels ranged from 30.6 % (1996) to 45.4 % (1993) across the years, with relatively lower no data pixels percentages recorded from 2014 to 2021 (less than 37.2 %; Fig. 3a). Generally, earlier years recorded higher no data pixels percentages compared to later years. For example, the monthly distribution (Fig. 3b) showed the least percentage of no data pixels for February (26.8 %) and the highest for October (51.2 %).

Due to the presence of no data pixels, it is necessary to inform the reader on the percentage coverage of LST pixels. LST pixel coverage for each image is calculated as the LST pixels retrieved divided by the total number of pixels for a given lake multiplied by 100 %. The LST pixel coverage is reported for each lake on a given day as part of the naming and metadata of our dataset. Figure 4 shows the yearly distribution of LST pixel coverage for the entire dataset. Lakes with less than 10 % of LST pixels on a given day were eliminated from the dataset. The percentage of lakes with LST pixel coverage greater than 90 % was 47.2 % (Fig. 4a). A greater percentage of lakes (77.4 %) in the dataset had more than 50 % LST pixel coverage. The percentage of lakes with LST pixel coverage greater than 90 % is plotted in Fig. 4b on an annual scale. Results show a general reduction in percentage with time, where earlier years had higher percentages of LST pixel coverage (>90 %) than recent years. This downward trend can be attributed to the Landsat 7 ETM+ SLC-off issue, which increases the presence of no data pixels.

Even though the typical overpass for Landsat is 16 d, the temporal resolution of the North Slave LST dataset varied due to the overlap of satellite sensors for specific years and the inability to retrieve LST due to the cloud cover. The distribution and frequency of the data were based on the operational times of the three Landsat satellites used in this study. Most of the dataset was derived from Landsat 5 (43 %). Landsat 7 and Landsat 8 contributed 34 % and 22 % of the dataset, respectively. LST images from 1999 were derived from two sets of Landsat data (Landsat 5 and Landsat 7 from 1999 to 2011; Landsat 7 and Landsat 8 from 2013 to 2021). Years with overlapping sensors may have shorter temporal resolution than years with only one sensor retrieval. As a re-

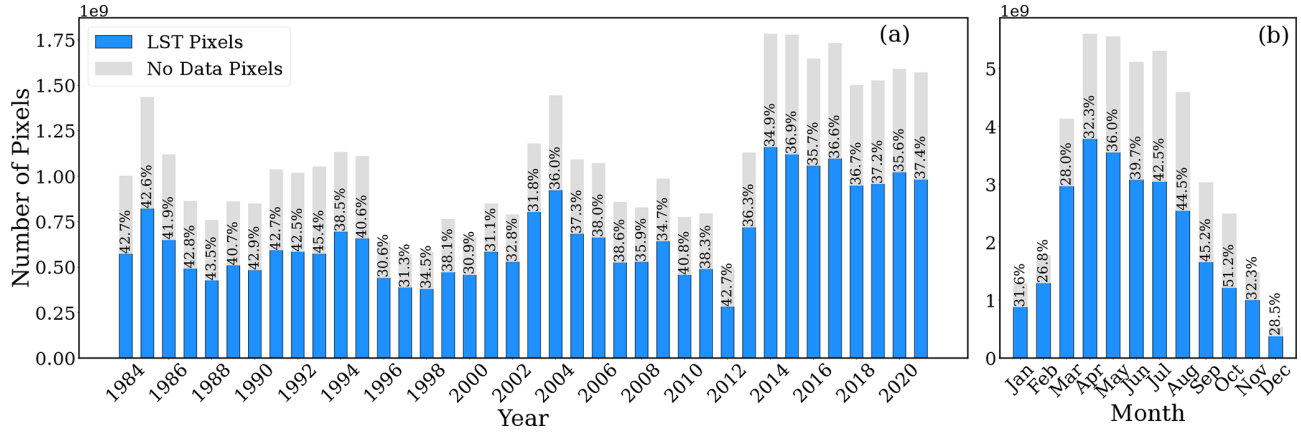

Figure 3. **(a)** Yearly and **(b)** monthly distribution of LST pixels vs. no data pixels, highlighting the percentage of no data pixels for a given period.

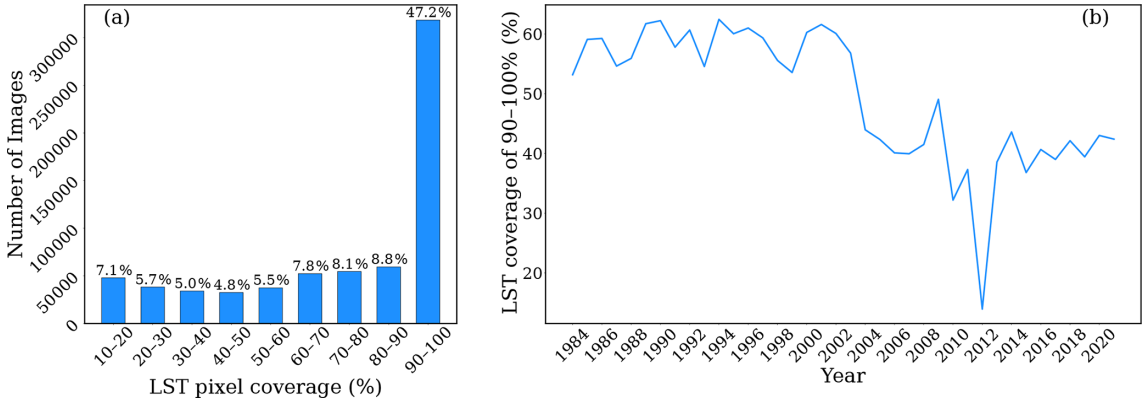

Figure 4. **(a)** Distribution of LST pixel coverage (%) and **(b)** yearly percentage of the dataset, with LST coverage ranging from 90 %–100 %.

sult, there is an inconsistency with the temporal resolution of the LST product.

4.2 North Slave LST evaluation

4.2.1 Evaluation of North Slave LST data

The accuracy of generated North Slave LST was examined by evaluating the Landsat-derived LST to corresponding in situ data (Fig. 5). Dates from measured in situ surface water temperature data (DataStream and ECCC) and derived North Slave LST data were matched. In addition, the widely used daily MODIS LST was compared with the generated dataset. Ground-based observations were compared against equivalent pixels within which measurements were taken, and the North Slave LST data were plotted against corresponding in situ surface temperature measurements (Fig. 5). A good correlation was observed between North Slave LST data and in situ surface water temperature, with an R^2 value of 0.89 for the regression line. The North Slave LST was slightly higher than in situ records, with a MBD of 0.12 °C and RMSD of 1.71 °C.

Statistical parameters, including average yearly LST for the open-water season, total average LST, and variance, were calculated for available ECCC and DataStream in situ data and compared against North Slave LST, which is highlighted in Table 2. Absolute differences calculated for the parameters ranged from 0.1 to 1 °C. The highest absolute difference for the average LST of open water between the two datasets was 1 °C calculated for the year 2000 of the ECCC data. The variance was 0.6 and 0.3 °C for the ECCC and DataStream data, respectively. Differences between the total LST average were the lowest, with 0.3 °C from 1999 to 2003 and 0.1 °C from 2014 to 2019.

Deviations between North Slave LST and measured surface water temperature could be due to differences between image acquisition times and the time of in situ measurements. The Landsat capture times of the NSR were between 18:00 and 20:00 UTC, corresponding to 12:00 and 14:00 LT (local time). However, the time of in situ observations was variable and did not necessarily correspond to the time of satellite image acquisition. Further variations in North Slave LST can also be attributed to the differences in sample collection and

Table 2. Comparison of yearly average LST, average LST, and variance between North Slave LST and in situ LST.

Statistical parameters	Data	Period	In situ LST (°C)	North Slave LST (°C)	Absolute difference (°C)
Average LST for open-water season (June–September)	ECCC	1999	11.9	12.2	0.3
		2000	10.8	11.8	1
		2001	13.7	14.2	0.5
		2002	11.1	11.2	0.1
		2003	12.2	12.5	0.3
	DataStream	2014	13.7	14.2	0.5
		2015	15.1	14.5	0.6
		2016	16.1	16.4	0.3
		2017	15	15.5	0.5
		2019	14.2	13.3	0.9
Total LST average for open-water season	ECCC	1999–2003	12.3	12.6	0.3
	DataStream	2014–2019	14.9	14.8	0.1
Variance	ECCC	1999–2003	15.5	14.9	0.6
	DataStream	2014–2019	3.8	4.1	0.3

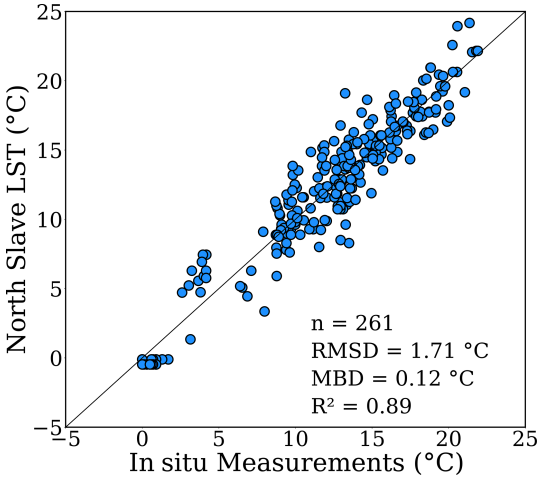

Figure 5. Comparison of North Slave LST with DataStream and ECCC in situ measurements of water surface temperature during open-water seasons.

spatial resolution. North Slave LST is essentially the mean of ∼ 60–120 m^2 area instead of a single in situ location. Possible errors reported by other studies for the differences in measured and Landsat values include georeferencing and radiometric and memory effects (Chander and Markham, 2003; Markham et al., 2014; Sentlinger et al., 2008; USGS, 2022; Young et al., 2017).

4.2.2 Yearly and monthly comparison of North Slave LST to MODIS LST

MODIS LST was first compared against available water surface temperature measurements from DataStream (Fig. 6a) and North Slave LST for days when records were available for all three data sources. The aim was to compare the deviation of North Slave LST and water surface temperature to that of MODIS LST and water surface temperature. A relatively low coefficient of determination was observed for MODIS LST ($R^2 = 0.5$) compared to the North Slave LST ($R^2 = 0.94$) when evaluated against measured water surface temperature. RMSD values were also higher for MODIS LST (4.63 °C) than North Slave LST (1.55 °C), with a MBD of 2.35 and −0.12 °C for MODIS LST and North Slave LST, respectively.

North Slave LST was further compared against MODIS LST from 2003 to 2021 (ice-covered and open-water areas separately) for larger study lakes (30 km^2) to avoid pixel mixing with land (Fig. 6b). Results showed a RMSD of 2.56 °C and MBD of 1.45 °C for ice-covered LST, suggesting an overestimation of North Slave LST during this period. On the other hand, an underestimation against MODIS LST was observed (MBD = −1.14 °C) for open-water LST with a relatively higher RMSD of 3.39 °C. This underestimation was expected as MODIS LST overestimates when compared against in situ data (Fig. 6a). Even though a prior comparison

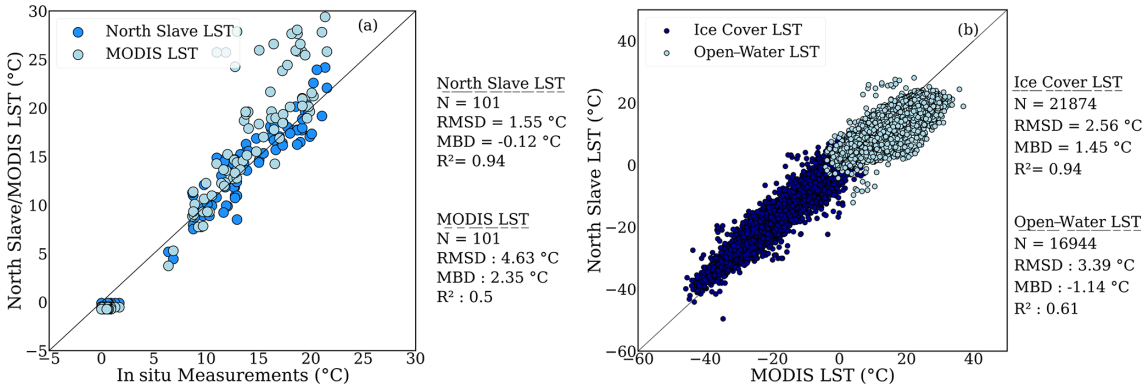

Figure 6. Comparison of North Slave LST and MODIS LST to **(a)** DataStream and ECCC in situ water surface temperature measurements during open-water seasons **(b)** MODIS LST during open-water and ice-covered seasons.

of MODIS LST to surface water temperature demonstrated a lower coefficient of determination, North Slave LST was still further compared against MODIS LST in this study. However, the decision to use MODIS for comparative analysis was due to the unavailability of continuous historical measurements of lake surface temperature. Additionally, MODIS LST provided an added outlook on the capability of North Slave LST to highlight historical trends despite the low temporal resolution by demonstrating a good correlation between the LST values ($R = 0.93$).

Figure 7a and b demonstrate the yearly and monthly RMSD values derived from the comparison between North Slave LST and MODIS LST. Yearly RMSD shows a generally decreasing RMSD from earlier to later years, which may be attributed to Landsat's sensor change in recent years. LST values derived from 2013 onwards were extracted from Landsat 8 OLI/TIRS, which is known to have improved signal-to-noise ratio and calibration, higher 12 bit radiometric resolution, and narrower spectral bands compared to previous sensors (Irons et al., 2012; Roy et al., 2014). Most importantly, Landsat 8 OLI/TIRS has a radiometric uncertainty of 3 %, compared to Landsat 7 ETM+ (5 %), and a reduced band saturation (Markham et al., 2014). Monthly RMSD comparing MODIS LST to North Slave LST showed that RMSDs were lowest in spring and highest in winter. LST in spring months (March–May) had the least deviation (RMSD = 1.9–2.9 °C) when compared against MODIS data.

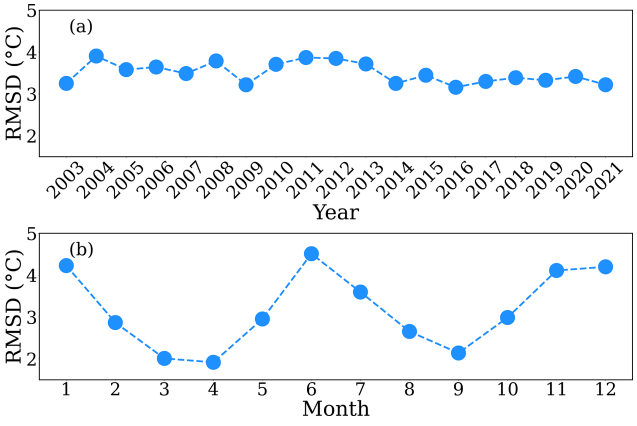

Figure 7. Yearly and monthly RMSD values from evaluating North Slave LST with MODIS LST from 2003 to 2021.

4.3 North Slave LST dataset distribution

4.3.1 Temporal distribution of North Slave LST dataset

LST was derived from the thermal radiation of the lakes' uppermost layer; hence; the skin temperature is given. A total of 673 223 gridded data files and 536 tabular data were included in the generated North Slave LST dataset (https://doi.org/10.5683/SP3/J4GMC2) for the 535 lakes studied across the NSR (Attiah et al., 2022). The yearly and monthly distribution of the dataset within and between lakes varied temporally and is highlighted in Fig. 8. Overall, the yearly distribution of the North Slave LST dataset was greater in recent years, with the period between 2014 and 2021 having the majority of the data and yearly percentages ranging from 4.15 % to 5 % of the total dataset. The larger number of data files in recent years was due to LST retrieval from a combination of Landsat 7 and Landsat 8 compared to the single-sensor retrieval (Landsat 5) for earlier years. As a result, the highest yearly percentage of the North Slave LST dataset was for 2014 (5 %), and the lowest yearly percentage was for 1988 (1.2 %). Unavailable data for the various years were predominantly due to insufficient usable Landsat data for winter months.

The monthly distribution of the North Slave LST dataset showed the month of May with the highest percentage (13.9 %) and December (1.3 %) with the lowest. Generally, colder months (October–April) had fewer data (42.7 %) compared to relatively warmer months (May–September; 57.3 %). Data are unevenly distributed across months and

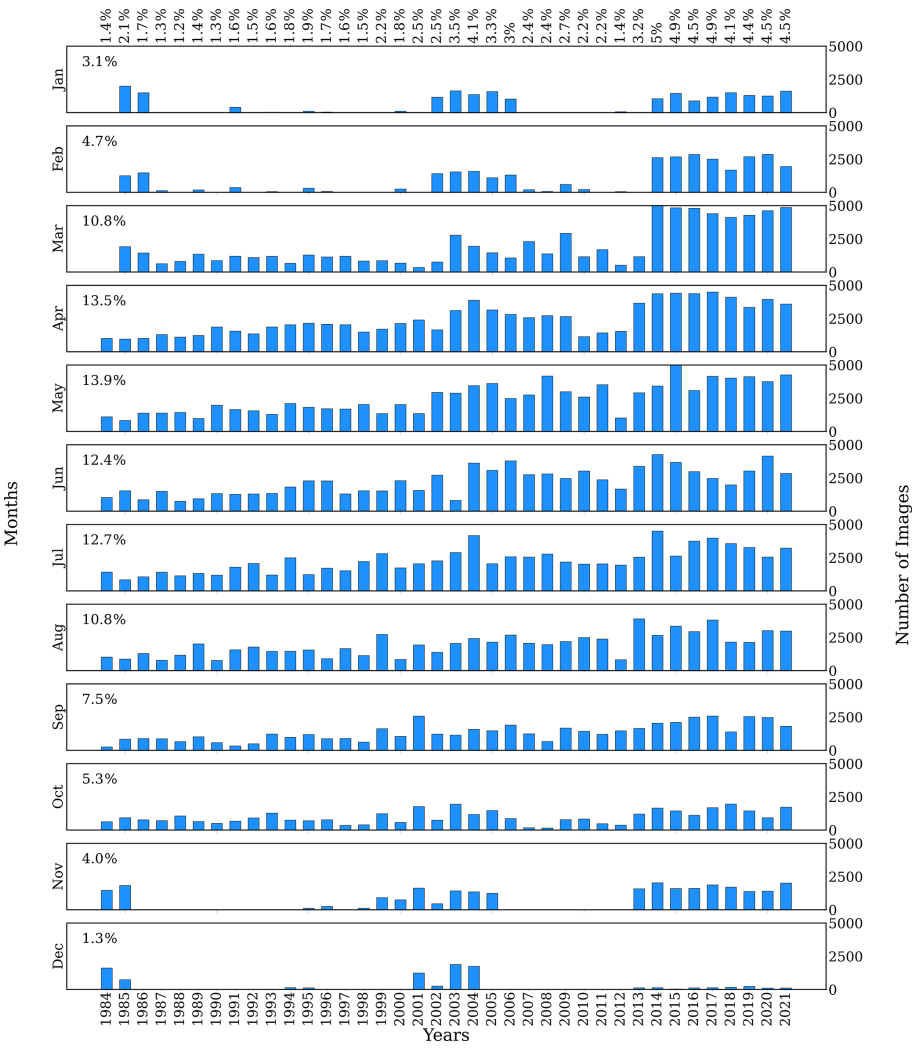

Figure 8. Yearly and monthly distribution of the North Slave LST dataset from 1984 to 2021. Percentages (%) represent the total percentage of the entire data for each month or year.

years due to differences in overpass times and influences like cloud cover and other atmospheric impacts on data retrieval.

4.3.2 Spatial dataset distribution of LST dataset between lakes

While study lakes are widely distributed across the NSR, a large number (144 out of 535) were within 150 km distance of Yellowknife. The average yearly number of images for each lake in the study region is demonstrated in Fig. 9. The average yearly minimum number of images was 20, reaching a maximum of 45. Lakes with a relatively smaller number of images were mainly distributed around Yellowknife. Smaller-sized lakes generally had fewer images than relatively larger ones, and this can be primarily attributed to clouds covering the entirety of small lakes. Most lakes (152 out of 535) had between 40 and 45 images, and 71 % of the total lakes in the dataset had more than 30 images per year. Lakes with fewer pixels are more likely to be entirely cloud covered and lose relatively more surface area due to the lake buffer.

4.4 North Slave LST dataset

4.4.1 NetCDF spatial coverage of LST

The North Slave LST dataset includes LST for 500 lakes with known names and 35 without names. NetCDF (Network Common Data Form) and tabular data are the data types in this dataset. NetCDF is a file format for storing multidimensional data and, hence, capturing the spatial coverage and dimension of LST for study lakes in this dataset. To facilitate easy data queries, each NetCDF filename includes the name of the lake, date, longitude, latitude, minimum LST, maximum LST, mean LST, number of pixels, and the percentage area of the LST pixels coverage of the lake for a given

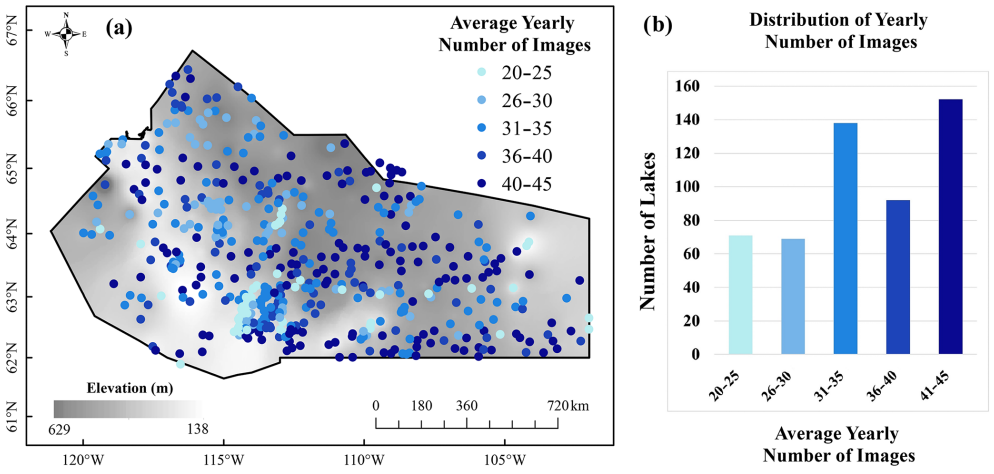

Figure 9. Distribution of the average yearly number of available images for lakes in the NSR.

day. The naming convention for lakes and their explanation is summarised in Table 3. The dataset was grouped based on the first alphabet of the lake name, then the name of the lake, and finally into yearly sub-groups.

The NetCDF files in our dataset have a two-dimensional variable, lst, which shows the spatial distribution of lake surface temperature. In addition, the one-dimensional x and y axes show the lake's extent and the number of pixels. The spatial reference for the data is the World Geodetic System 1984, EPSG:4326, with a 30 m resolution.

4.4.2 Tabular data of LST

The second type of data included in the North Slave LST dataset is the tabular data containing LST statistics on individual study lakes for a given day. Derived attributes include the minimum, maximum, median, mean, number of ice cover pixels, number of open-water pixels, percentage of lake captured, and other lake properties. Table 4 highlights the column and field names from the tabular data and what they represent. These tabular data are generated for each lake and are included in the dataset. Each filename consists of the lake name followed by longitude and latitude, for easy query, based on location (e.g. AcastaLake_-115.564_65.3783). Additionally, monthly means were calculated for each lake and combined into one file in the dataset.

4.5 Spatial patterns of North Slave LST

4.5.1 Seasonal lake spatial distribution of North Slave LST

The seasonal spatial distribution of mean LST from 1984 to 2021 is shown in Fig. 10 to highlight the spatial variation in LST for different seasons. The distribution of average LST was computed for winter (December–January), spring (March–May), summer (June–August), and autumn (September–November) for all study lakes. LST on lakes in the NSR is generally negative in winter (−26 to −18 °C) and spring (−17 to −3 °C). This is because lakes are ice covered during these two seasons, constituting negative LST values. Autumn was characterised by both positive and negative LST values (−8 to 3 °C). Lakes start to freeze in autumn, and the freezing rate is influenced by several factors, resulting in differences in the open-water duration, which affect the average temperature. The average LST for summer ranged from 6 to 22 °C. Winter had the lowest LST ranges with a variability of 8 °C, while LST variability for summer was twice (16 °C) that of winter. This is expected, as temperatures on lakes during this season are influenced by several factors, including lake size, elevation, depth, latitude, longitude, and volume (O'Reilly et al., 2015; Xie et al., 2022), in addition to air temperature. Seasonal LST spatial distribution provides insight into the climate patterns of the NSR region.

4.5.2 Spatial distribution of North Slave LST for 2021

The spatial distribution of the mean annual LST across the NSR for 2021 is shown in Fig. 11a, which highlights the remarkable spatial differences between lakes at higher versus lower elevations, with lower-elevation lakes generally demonstrating higher LST. Based on the mean annual LST values in 2021, the LST category was divided into five different ranges, as shown in the map (−12 to −9 °C, −9 to −6 °C, −6 to −3 °C, −3 to 0 °C, and 0 to 3 °C). Figure 11b shows most lakes (28 %), with a mean of −3 to 0 °C. The lake distribution of mean LST was 8 %, 22 %, 27 %, 28 %, and 15 % from colder to warmer LST categories, respectively. The percentage of the total area covered by lakes in relation to mean LST was 34 %, 27 %, 18 %, 19 %, and 2 %, respectively (Fig. 11b). Although the number of lakes with LST ranging from −12 to −9 °C was the least (8 % of lakes), the percentage of the total area covered by lakes with this LST range was the largest (34 % of lakes). The total area covered

Table 3. Sections of North Slave LST dataset's NetCDF filename and description.

Sample lake file name: AcastaLake_19840428_-115.564_65.3783_-5.90_-7.10_-6.50_17482_099.nc	
Section	Description of the section
Lake name: AcastaLake	The lake's name predominantly derived from the Water File – Lakes and Rivers (polygons) data from Statistics Canada. Lakes' unknown names were prefixed with NoNameLake and a number.
Date 19840428	The date of the LST is in the format YYYYMMDD. It represents the date that the Landsat scene was captured over the lake.
Longitude (°): −115.564	The longitude represents a known longitude predominantly located at the lake's centre when plotted against the latitude in decimal degrees.
Latitude (°): 65.3783	The latitude represents a known latitude predominantly located at the lake's centre when plotted against the longitude in decimal degrees.
Maximum temperature (°C): −5.90	The maximum LST value retrieved on the lake for the given date.
Minimum temperature (°C): −7.10	The minimum LST value retrieved on the lake for the given date.
Mean temperature (°C): −6.50	The mean LST value calculated from all LST pixels retrieved on the lake for the given date.
Number of LST pixels: 17 482	The number of LST pixels retrieved on the lake for the given date.
LST pixels coverage (%): 099	The number of LST pixels retrieved from the lake for the given date is divided by the total number of pixels representing the lake.

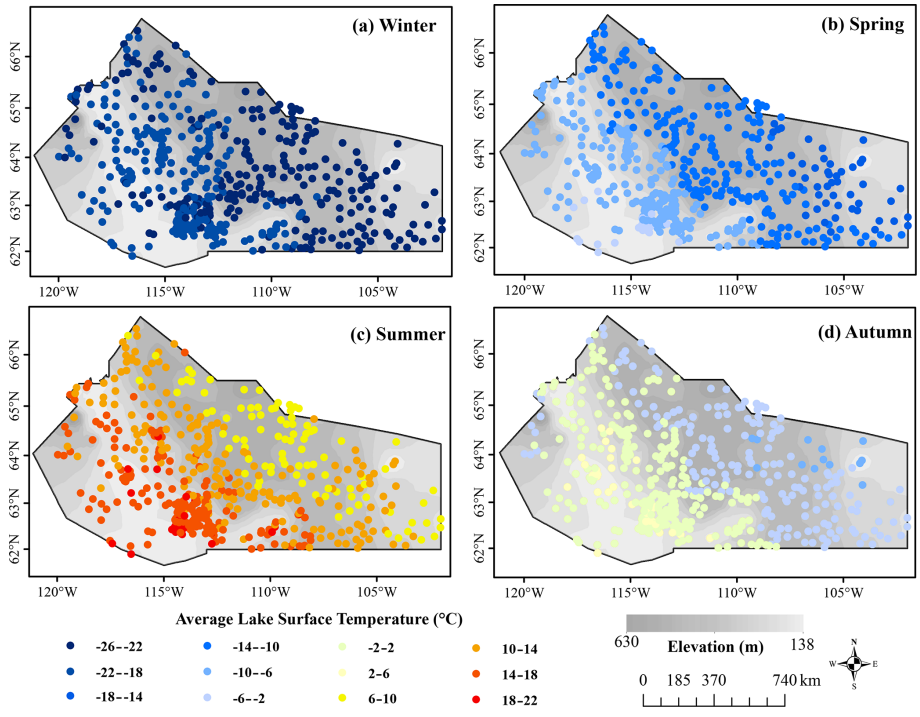

Figure 10. Spatial distribution of average LST of all years across the NSR for **(a)** winter, **(b)** spring, **(c)** summer, and **(d)** autumn.

Table 4. Column names of the tabular dataset and the description.

Column	Description
Lake_Name	The name of the lake from which the lake surface temperature was retrieved. The name of the lake was predominantly derived from the Water File – Lakes and Rivers (polygons) data from Statistics Canada. Lakes' unknown names were prefixed with NoNameLake and a number.
Date	The date which the lake surface temperature (LST) represents.
Year	The year of the LST in the format YYYY.
Month	The month of LST in the format MM.
Day	The day of LST in the format YY.
Maximum_Temperature	The maximum LST recorded on the lake in degrees Celsius (°C) at a given time.
Minimum_Temperature	The minimum LST recorded on the lake in degrees Celsius (°C) at a given time.
Median_Temperature	The median LST from all available pixels in degrees Celsius (°C).
Mean_Temperature	The mean LST from all available pixels in degrees Celsius (°C).
Total_Pixels	The total number of pixels representing the lake.
LST_Pixels	The number of pixels with LST values retrieved from the lake.
Percentage_LST_Pixels	The total percentage of pixels with LST values captured from the lake. Values are rounded to the nearest 1.
Count_Water_Pixels	The number of LST pixel values greater than 0 retrieved from the lake at a given time.
Count_Ice_Pixels	The number of LST pixel values less than 0 retrieved from the lake at a given time.
Percentage_Ice_Pixels	The Total percentage of ice pixels captured from the lake at a given time. Values are rounded to the nearest 1.
Landsat_Row_Path	The tile name, row, and path of the Landsat from which LST was retrieved.
Lake_Area	The surface area of the lake in square kilometres (km^2).
HyLak_ID	The ID is derived from the HydroLAKES dataset. Lakes with no ID are indicated with 0.
HyLak_Depth	The average depth of the lake derived from the HydroLAKES dataset in metres (m).
HyLak_Volume	The volume of the lake derived from the HydroLAKES dataset is million cubic metres ($1\,mcm = 0.001\,km^3$).
HyLak_Elevation	The elevation of the lake surface derived from HydroLAKES dataset in metres above sea level.
Long(m)	The longitude point on the lake in metres.
Lat(m)	The latitude point on the lake in metres.
Long(DD)	The longitude point on the lake in decimal degrees.
Lat(DD)	The latitude point on the lake in decimal degrees.
Monthly_Mean_Temperature	The mean LST on the lake for a given month.

for all lakes with mean LST from 0 to 3 °C was only 2 %. This suggests that several of the lakes with warmer temperatures were smaller sized. Generally, relatively warmer lakes were also distributed around Yellowknife and the southwestern part of the region.

4.5.3 Intra-lake spatial distribution of generated LST

Lakes in several studies are treated as homogenous entities; however, there is spatial variability in the surface temperature of a given lake based on several factors, including the difference in morphometry or the biological, physical, and anthropogenic activities occurring on the lake at a given time (Crosman and Horel, 2009; Huang et al., 2017;

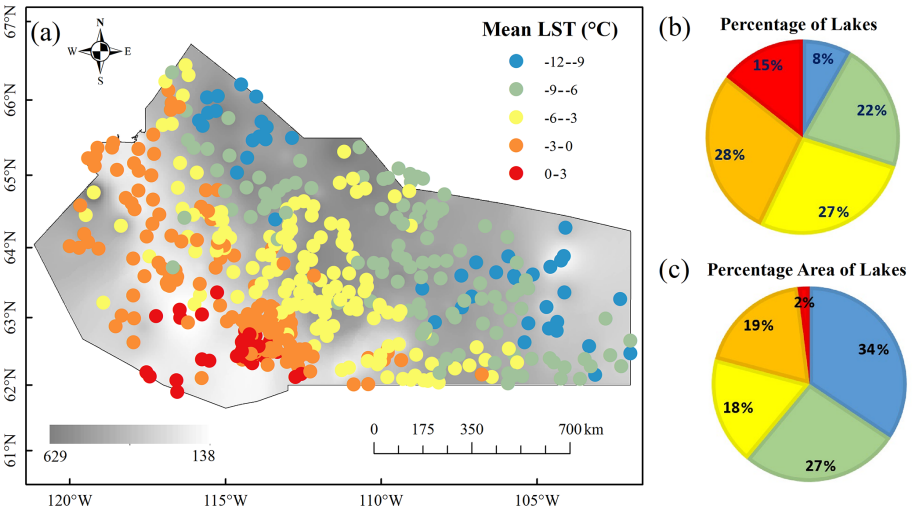

Figure 11. **(a)** Spatial distribution of mean LST for the year 2021 across the NSR showing **(b)** the percentage number of lakes and **(c)** the percentage area of lakes within specific LST ranges.

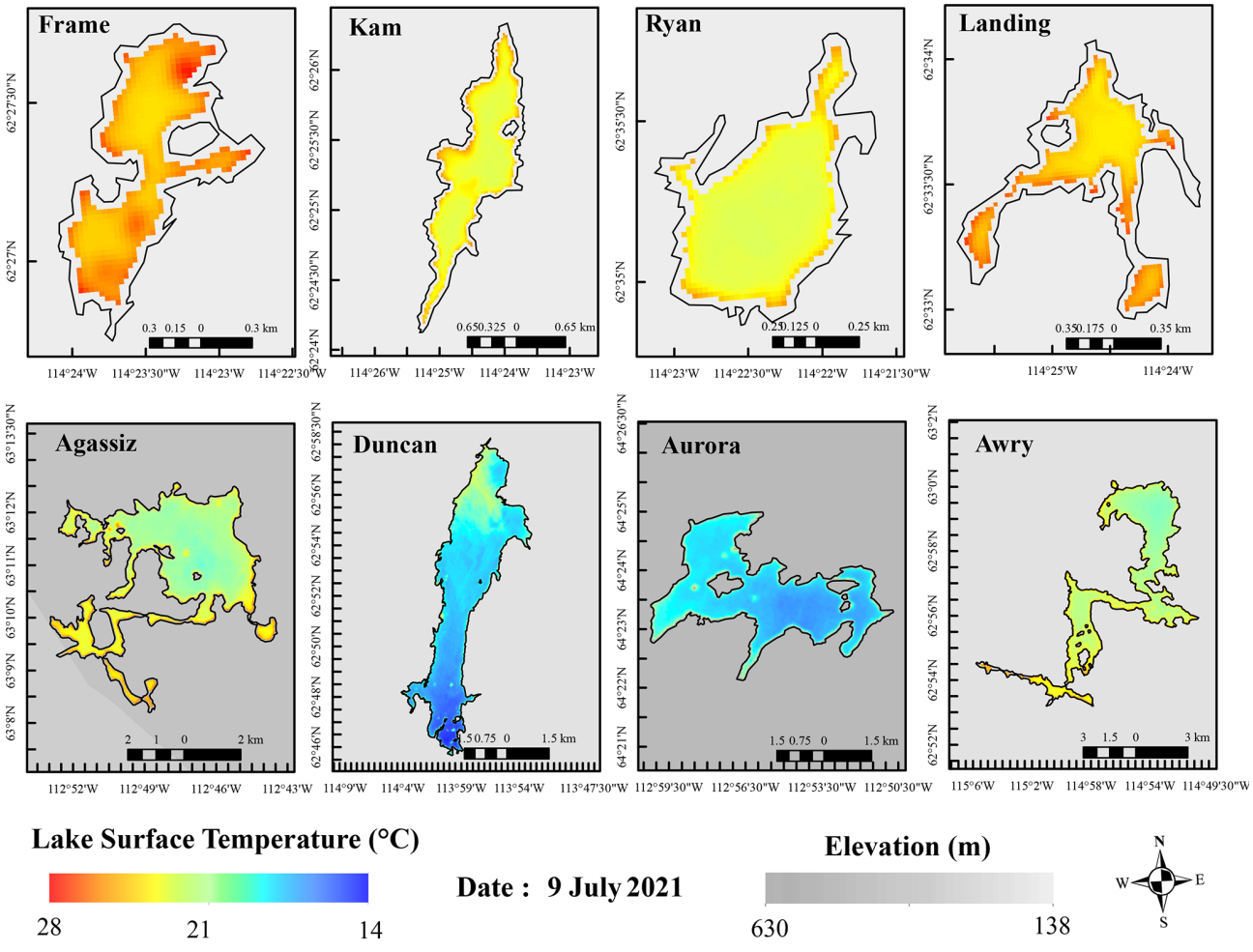

Figure 12. Intra-lake spatial distribution of LST on selected lakes in the NSR highlighting the North Slave LST's ability to capture small-scale details of the LST.

Yang et al., 2020). The North Slave LST dataset generated in this study can highlight the spatial variability within a given lake. As expected, the high spatial resolution and multidate LST generated show lakes' surface temperature heterogeneity. The phenomenon is demonstrated with LST distribution on 9 July 2021 for a few selected lakes within our study given as examples (Fig. 12).

Lakes may demonstrate significant surface temperature variations for various reasons, including wind redistribution, depth, and biological and anthropogenic activities. Warmer LSTs are generally at the shallower coastal regions of lakes; however, internal LST variations differ. An example is Duncan Lake (Fig. 12), which demonstrated warmer temperatures in the northern part of the lake than in the south. Maximum and minimum LST on lakes also differ, with some lakes having wider variations (e.g. Duncan Lake; 23–14 °C) and others having less variation (e.g. Frame Lake; 28–24 °C). Lakes' physical differences, location, and elevation may contribute to the different ranges of surface temperature distribution on individual lakes.

5 Data availability

The long-term (1984–2021) continuous high-resolution (30 m spatial resolution) regional (North Slave Region, NWT) gridded LST dataset is available at https://doi.org/10.5683/SP3/J4GMC2 (Attiah et al., 2022). The Landsat imagery used to generate this dataset can be downloaded from the USGS platform. Physical properties and names of lakes were derived from HydroLAKES (https://www.hydrosheds.org/products/hydrolakes, HydroSheds, 2022; Messager et al., 2016), Water File – Lakes and Rivers (polygons) data (https://www12.statcan.gc.ca/census-recensement/2011/geo/bound-limit/files-fichiers/ghy_000c06a_e.zip, Statistics Canada, 2022) and CanVec Series (https://open.canada.ca/data/en/dataset/9d96e8c9-22fe-4ad2-b5e8-94a6991b744b, Natural Resources Canada, 2019). Evaluation data were derived from Mackenzie DataStream (https://mackenziedatastream.ca/, last access: 25 May 2022, https://doi.org/10.25976/gm49-2a19, Environment and Climate Change Canada, Université de Montréal, 2020). ERA5 reanalysis data were obtained from Copernicus Climate Change Service (https://doi.org/10.24381/cds.adbb2d47; Hersbach et al., 2019).

6 Conclusions

A new gridded dataset (North Slave LST) containing lake surface temperature across the NSR, generated by applying a retrieval algorithm to the thermal bands of Landsat archives, was presented in this study. LST data are available for 38 years (from 1984 to 2021) on a 30 m spatial resolution and varying temporal resolution. North Slave LST dataset has proven that it is suitable for capturing small-scale details of LST on small lakes and is comparable with LST products like MODIS (1 km resolution) and other water surface temperature measurements.

The North Slave LST dataset includes 673 223 NetCDF gridded data files for all lakes, with a greater percentage (57.3 %) highlighting LST in warmer months. Tabular LST data have also been generated to report the aggregated values of LST on lakes. A high percentage (43 %) of the dataset was derived from Landsat 5. Lakes had a 100 m buffer applied, resulting in a pixel representation ranging from 16.7 % to 97.34 % of the lake area. Most of the dataset (77.4 %) had LST pixel coverage greater than 50 %, of which 42.2 % had pixel coverage greater than 90 %. Each lake's average yearly number of LST images was between 20 and 45.

The algorithm, when successfully applied, retrieves LST from Landsat images across the NSR, with a RMSD of 1.7 °C and MBD of 0.12 °C. The dataset produced provides continuous data and highlights spatial and temporal LST of lakes in the NSR. Based on generated North Slave LST, warmer lakes are predominantly located around Yellowknife and on the southwestern part of the NSR. Seasonal average LST is highlighted using the North Slave LST dataset, with summer having the highest variation in LST (16 °C) between lakes across the NSR. Intra-lake variability is also demonstrated in this dataset. The North Slave LST dataset will be continually updated with improved retrieval algorithms and up-to-date data as they become available.

Appendix A

Table A1. Properties of selected lakes in the North Slave Region.

Lake name	Latitude (°)	Longitude (°)	Area (km^2)	Elevation (m)	Average depth (m)	Number of pixels	Percentage of lake represented
Acasta Lake	−115.564	65.3783	18.23	399	4.7	17 645	87.11
Achilles Lake	−110.906	64.963	27.84	403	16.7	27 536	89.01
Acres Lake	−108.688	62.7499	3.36	333	9.6	2438	65.18
Agassiz Lake	−112.788	63.1797	19.89	338	17.9	18 113	81.95
Ajax Lake	−110.58	64.9737	24.32	446	8.2	23 524	87.05
Alexander Lake	−108.117	62.2884	6.24	385	6.8	5427	78.21
Alexie Lake	−114.083	62.6779	4.24	218	6	3357	71.23
Allan Lake	−113.063	62.9208	4.35	273	8	3893	80.46
Ambush Lake	−113.824	65.7125	16.02	413	13.6	15 379	86.39
Angelique Lake	−113.421	64.6265	17.84	403	10.2	16 742	84.47
Angle Lake	−114.177	62.8313	4.11	195	21.1	3404	74.45
Anton Lake	−114.461	62.9713	3.34	253	8.8	2404	64.67
Ardent Lake	−115.736	65.6577	14.28	412	6.2	14 331	90.34
Armi Lake	−114.124	63.7112	26.59	354	9.6	25 165	85.18
Arno Lake	−113.533	63.0506	0.11	–	–	43	36.36
Artillery Lake	−107.871	63.1744	521.89	352	24.3	552 430	95.27
Athenia Lake	−111.516	63.6452	42.29	416	7.2	38 069	81.01
Augustus Lake	−116.686	66.3619	9.78	340	22.3	9027	83.03
Aurora Lake	−112.921	64.3918	15.25	377	5.3	14 892	87.8
Awry Lake	−114.922	62.9506	26.89	201	19.7	25 545	85.5
Axecut Lake	−104.138	63.8762	1.95	165	5.6	1789	82.56
Aylmer Lake	−108.53	64.1244	680.73	355	19.7	715 690	94.62
Back Lake	−109.329	63.8188	86.59	384	12.9	87 319	90.76
Back River	−108.275	64.609	62.66	333	15.6	61 472	88.29
Baldhead Lake	−113.634	64.6092	20.02	409	11.2	19 439	87.41
Banting Lake	−114.285	62.6292	3.86	171	10.9	2959	68.91
Barnston Lake	−110.033	63.1483	12.64	384	15	11 950	85.13
Bartlett Lake	−118.336	63.0863	183.8	260	4.4	191 259	93.65
Basile Lake	−111.261	62.2174	15.19	171	20.2	15 196	90.06
Basler Lake	−115.945	63.9303	99.21	230	40.3	99 610	90.36
Baton Lake	−115.096	64.3761	1.83	327	11.8	1089	53.55
Bear Lake	−114.184	62.3801	1.7	173	3.9	1158	61.18
Beauparlant Lake	−112.177	64.5722	13.62	445	6.6	12 519	82.75
Beauregard Lake	−114.336	62.7216	1.46	207	7.6	1220	75.34
Beaverhill Lake	−104.373	62.8032	121.51	278	12.9	129 356	95.81
Beaverlodge Lake	−118.194	64.6873	65.31	175	6.7	64 188	88.46
Beck Lake	−104.613	62.8365	4.82	282	1.8	4839	90.46
Bedford Lake	−109.496	62.9993	25.91	306	15.8	23 905	82.86
Bell Lake	−114.334	62.8427	3.82	226	7.1	3104	73.04
Benoit Lake	−116.251	66.3525	25.65	379	6.6	24 857	87.21
Bessonette Lake	−114.741	63.6612	8.57	296	10.2	7970	83.66
Betty Ray Lake	−116.574	63.5419	6.07	196	6.1	4935	73.15
Bewick Lake	−105.718	62.4994	85.96	341	8.4	83 936	87.88
Big Lake	−112.986	64.857	65.63	407	7.8	66 426	91.09
Big Rocky Lake	−102.294	62.2768	78.01	254	8.1	75 539	87.16
Bighill Lake	−114.036	62.5076	4.58	189	6.2	4342	85.37
Biologist Lake	−104.087	64.2761	3.48	300	2.5	3336	86.21
Birch Lake	−116.565	62.067	85.93	187	5.7	89 784	94.04
Bishop Lake	−116.157	65.5005	46.4	347	14.8	47 643	92.41
Black Lichen Lake	−116.263	64.4217	58.82	287	23.7	58 221	89.07
Blaisdell Lake	−113.579	62.7784	5.95	249	6.6	5191	78.49
Blake Lake	−106.448	62.1172	12.76	389	5.3	11 905	83.93
Bodie Lake	−105.853	62.9572	14.88	341	5.6	14 557	88.04
Boland Lake	−115.69	64.5396	28.93	255	33.6	26 869	83.44
Boulder Lake	−113.074	63.7656	16.91	361	13.2	16 609	88.35

Table A1. Continued.

Lake name	Latitude (°)	Longitude (°)	Area (km^2)	Elevation (m)	Average depth (m)	Number of pixels	Percentage of lake represented
Box Lake	−109.423	63.9199	39.37	384	12.9	38 395	87.78
Bras d'Or Lake	−115.743	62.3927	33.03	–	–	34 349	93.58
Breadner Lake	−116.749	65.8623	27.34	295	19.7	27 433	90.31
Breithaupt Lake	−105.407	62.6386	19.67	335	2.9	18 063	82.66
Bridge Lake	−112.276	63.268	3.58	395	6.9	3013	75.7
Brock Lake	−112.833	62.4155	0.17	255	3.1	81	41.18
Broken Dish Lake	−116.267	65.8579	3.91	368	11.9	3721	85.68
Brown Water Lake	−115.863	64.5998	51.97	275	35	45 575	78.7
Buckham Lake	−112.647	62.2974	30.98	189	19.6	28 839	83.8
Bunting Lake	−109.783	62.4827	0.23	235	2.9	167	65.22
Burbanks Lake	−108.6	62.7652	0.08	–	–	37	37.5
Burke Lake	−116.712	63.5178	2.37	170	7.9	2074	78.9
Bustard Lake	−108.415	64.3342	7.41	372	10.8	7067	85.83
Calder Lake	−115.234	65.8658	15.31	454	6.8	14 620	85.83
Calypso Lake	−115.844	65.7256	12.98	380	12.4	11 701	81.12
Campbell Lake	−106.894	63.2391	110.9	373	7.8	105 646	85.73
Camsell Lake	−111.185	63.6228	158.16	411	12.6	153 622	87.42
Carey Lake	−102.909	62.2067	255.34	265	12.1	259 064	91.24
Caribou Lake	−114.023	62.986	2.78	245	4.9	2077	67.27
Carter Lake	−104.303	62.9554	29.59	274	8.1	27 590	83.91
Cassino Lake	−119.398	64.0755	22.44	325	4.4	23 561	94.47
Castor Lake	−115.978	64.4679	35.74	284	28.6	34 101	85.87
Chan Lake	−114.355	62.6408	0.41	236	2.8	238	51.22
Chan Lake	−116.542	61.8909	0.84	239	6.5	701	75
Chartrand Lake	−115.532	64.4607	20.79	336	16.7	19 626	84.94
Chedabucto Lake	−115.553	62.3691	43.01	193	5.7	44 908	93.98
Chelay Lake	−119.403	65.2223	1.72	199	5.6	1393	72.67
Chipp Lake	−112.626	62.4685	2.9	270	2.1	2056	63.79
Chitty Lake	−114.123	62.7149	2.38	221	6.2	1822	68.91
Clinton Colden Lake	−107.474	63.9586	599.71	352	13.4	608 092	91.23
Clive Lake	−118.906	63.212	64.84	255	3.6	66 713	92.47
Coldblow Lake	−104.107	63.361	12.1	320	3.8	11 726	87.19
Cole Lake	−116.594	63.6731	9.24	194	11.9	8010	77.92
Compton Lake	−109.79	62.5331	8.91	246	26.2	9010	91.02
Consolation Lake	−112.797	62.5081	20.01	238	14.8	15 423	69.37
Contwoyto Lake	−110.506	65.3085	163.62	435	22.2	166 125	91.38
Cook Lake	−108.849	63.1595	49.99	352	10.2	45 458	81.84
Cooley Lake	−109.052	62.0574	9.33	336	10	8220	79.31
Cosmos Lake	−104.224	63.8148	2.14	150	8.9	2052	85.98
Cotterill Lake	−114.847	64.1539	17.93	334	10.9	16 688	83.77
Courageous Lake	−111.188	64.1657	228.32	395	12.6	232 082	91.48
Courier Lake	−111.946	63.5337	1.46	439	3.8	1092	67.12
Cowan Lake	−115.274	63.3612	4.44	218	9.7	3373	68.47
Crapaud Lake	−114.021	62.9358	5.87	225	5.3	4945	75.81
Credit Lake	−112.492	64.6574	17.7	429	3.2	16 740	85.14
Creek Lake	−114.01	62.4733	0.88	–	–	774	79.55
Criss Lake	−113.514	63.0824	0.11	320	2.4	51	45.45
Croft Lake	−104.216	62.1037	15.74	337	6.4	14 405	82.34
Crooked Foot Lake	−113.554	64.1502	9.02	374	8.2	8807	87.92
Cruikshank Lake	−105.357	63.5315	10.7	313	4.7	10 138	85.23
Danes Lake	−111.706	63.2228	2.79	426	6.5	2398	77.42
Daoust Lake	−108.915	62.1353	11.25	333	10.9	11 028	88
Daran Lake	−115.06	64.0299	20.75	257	37.7	19 570	84.87
Darrell Lake	−105.65	63.7836	21.19	341	6.7	17 950	76.26
Dauphinee Lake	−114.721	63.8824	9.95	288	13	9300	84.12
David Lake	−114.378	62.5436	0.13	198	2.7	55	38.46
Davis Lake	−115.439	64.3984	1.33	335	10.8	1029	69.92
Day Lake	−113.504	62.6637	0.83	264	3.6	610	66.27
Defeat Lake	−113.643	62.3382	18.42	192	6.8	17 144	83.77
Delmar Lake	−112.055	63.1382	8.65	406	8.1	7885	82.08
Denis Lake	−112.595	63.3542	7.34	387	9.2	6569	80.52
Desperation Lake	−112.401	62.5781	26.04	244	21.9	25 205	87.1

Table A1. Continued.

Lake name	Latitude (°)	Longitude (°)	Area (km^2)	Elevation (m)	Average depth (m)	Number of pixels	Percentage of lake represented
Desert Lake	−115.76	62.0993	7.68	202	4	7831	91.8
Devore Lake	−112.902	62.5951	0.94	270	4.5	738	70.21
Devreker Lake	−117.318	64.6627	13.12	235	24.8	12 774	87.5
Dissension Lake	−113.499	63.983	4.97	336	5.3	4354	78.87
Dodds Lake	−113.424	63.1327	4.68	309	3.9	4020	77.35
Dome Lake	−113.255	62.7624	2.7	250	4.4	2166	72.22
Doodad Lake	−112.755	62.3539	0.27	257	2.1	133	44.44
Dorothy Lake	−112.534	62.4523	3.45	275	3	2744	71.59
Doyle Lake	−109.108	63.0974	13.79	352	13.4	12 146	79.26
Drumlin Lake	−114.32	64.8287	36.46	437	5.4	34 338	84.75
Drybones Lake	−112.405	63.5129	33.07	411	10.5	32 593	88.69
Drygeese Lake	−114.166	62.734	3.74	217	7	3313	79.68
Driedmeat Lake	−112.891	64.2536	7.92	379	6.7	7381	83.84
Duck Lake	−114.239	62.4336	5.38	155	6.6	4604	76.95
Duckfish Lake	−114.44	62.6736	5.79	228	5.3	4973	77.37
Dumas Lake	−116.301	66.4878	22.91	351	9.5	21 601	84.85
Dumbell Lake	−111.083	64.0315	4.15	433	5.2	3571	77.35
Duncan Lake	−113.96	62.8705	68.2	214	21.4	70 900	93.56
Egg Lake	−114.029	62.4897	0.91	192	3.7	638	62.64
Eileen Lake	−107.639	62.2437	135.71	369	9.6	128 076	84.94
Elk River	−105.359	62.2166	59.41	337	4.4	49 250	74.62
Ellington Lake	−117.32	65.0299	26.54	248	16.7	25 216	85.49
Ernie Lake	−102.352	63.2671	20.99	252	12.2	21 080	90.38
Etna Lake	−119.484	64.4488	45.73	356	3.3	46 177	90.88
Eyeberry Lake	−104.696	63.1425	81.6	201	5.1	82 207	90.67
Eyston Lake	−116.417	65.1823	23.89	298	27	22 348	84.18
Faber Lake	−117.297	63.9325	383.34	203	22	402 498	94.5
Face Lake	−110.126	62.3145	2.47	371	6.2	1750	63.56
Fairbairn Lake	−111.006	62.2618	14.6	169	12.8	14 698	90.62
Fat Lake	−111.64	63.3964	12.85	412	7.5	11 492	80.47
Faulkner Lake	−112.275	62.1985	2.37	204	9.6	1906	72.57
Fawn Lake	−117.529	62.1864	24.82	179	3.3	25 619	92.91
Fenton Lake	−112.953	63.0183	16.2	277	23.1	15 743	87.47
Fenwick Lake	−119.1	65.3622	3.14	205	11.1	2890	82.8
Fiddlers Lake	−114.509	62.468	0.28	192	2.2	196	64.29
Finger Lake	−114.357	62.5751	0.05	–	–	10	20
Fishhook Lake	−115.236	64.0626	8.4	262	19.2	7584	81.31
Fletcher Lake	−108.763	63.5923	164.24	388	11.6	164 217	89.99
Forcier Lake	−116.351	66.0568	10.1	371	9.5	9373	83.56
Ford Lake	−107.409	63.1433	35.02	389	4	33 188	85.29
Fortune Lake	−115.183	64.4511	0.36	353	4.4	232	58.33
Fox Lake	−114.417	62.483	0.52	199	2.7	359	61.54
Frame Lake	−114.391	62.4542	0.85	186	3.4	523	55.29
François Lake	−112.373	62.461	24.16	269	6.1	24 259	90.36
Frodsham Lake	−113.604	63.6462	23.34	336	11.8	23 316	89.8
Gagnon Lake	−110.45	62.0308	22.99	317	19.8	19 590	76.69
Gale Lake	−115.268	63.9338	1.1	277	7.6	863	70.91
Gamey Lake	−115.204	64.1352	0.54	328	5.5	370	61.11
Gar Lake	−114.373	62.5212	0.28	182	2.9	188	60.71
Garde Lake	−106.268	62.832	104.05	–	–	99 319	85.91
Gardenia Lake	−105.893	62.0199	40.35	361	5	36 955	82.43
Georic Lake	−112.984	63.1825	0.6	324	6.2	398	60
Germaine Lake	−114.609	63.2969	22.84	265	16.2	20 542	80.95
Ghost Lake	−115.147	63.8504	62.93	275	34.9	59 083	84.49
Giauque Lake	−113.831	63.1809	16.46	252	22.8	15 472	84.57
Glowworm Lake	−109.24	64.6365	102.5	412	20.4	102 052	89.61
Gold Lake	−107.949	64.7369	2.87	325	14.4	2113	66.2
Goodspeed Lake	−109.465	63.098	57.92	319	24.2	53 085	82.49
Goodwin Lake	−114.088	63.0453	2.82	248	7.4	2484	79.43
Gordon Lake	−113.201	63.0668	167.16	284	11.5	157 999	85.07
Grace Lake	−112.564	62.1628	3.7	218	5.7	3093	75.14
Grace Lake	−114.448	62.4188	0.64	172	3.4	378	53.12

Table A1. Continued.

Lake name	Latitude (°)	Longitude (°)	Area (km^2)	Elevation (m)	Average depth (m)	Number of pixels	Percentage of lake represented
Graham Lake	−113.807	62.9008	16.37	216	17.8	16 453	90.47
Gras Lake	−110.448	64.523	705.63	404	9.6	724 732	92.44
Great Slave Lake	−113.243	62.2183	9553.89	148	59.1	8 607 738	53.14
Greenrock Lake	−116.512	65.9309	2.8	394	7.8	2399	77.14
Greyling Lake	−114.289	62.6827	0.5	198	5.9	274	50
Grizzly Bear Lake	−112.982	64.1998	21.13	376	5.6	20 776	88.36
Grizzly Lake	−115.574	64.5081	4.6	327	11.9	4108	80.43
Grodsky Lake	−108.391	62.082	5.87	372	3.7	5652	86.54
Hair Lake	−110.048	62.4313	5.24	185	16.8	4952	85.11
Hanbury Lake	−105.698	63.5646	7.57	328	8	7295	86.79
Handle Lake	−114.397	62.4914	0.21	196	2.3	116	47.62
Handley Page Lake	−116.777	65.9876	29.03	315	17.3	28 307	87.77
Hansen Lake	−116.748	65.6957	16.33	323	17.6	15 363	84.69
Harald Lake	−113.535	62.685	4.12	260	3.3	3060	66.75
Hardisty Lake	−117.676	64.5506	302.59	186	26.9	298 804	88.86
Harrison Lake	−107.659	63.0102	4.71	402	3.9	3464	66.24
Havant Lake	−115.555	65.8333	9.79	401	7.8	9524	87.33
Haywood Lake	−110.504	63.4599	32.79	395	8.2	32 691	89.72
Healey Lake	−106.663	64.2964	153.4	352	8.2	141 117	82.67
Heuss Lake	−107.081	63.3052	9.63	360	6.1	7831	73.21
Hidden Lake	−113.682	62.5107	0.2	193	5	104	45
Hidden Lake	−113.556	62.5531	12.45	205	14.7	12 189	88.11
Hilltop Lake	−111.041	63.3671	25.91	407	5.7	23 714	82.36
Hislop Lake	−116.927	63.5189	34.04	172	14.6	33 779	89.28
Hoare Lake	−105.131	63.6208	8.66	305	5	7769	80.72
Holmason Lake	−115.024	63.9889	1.27	269	13.9	1065	75.59
Homer Lake	−114.286	62.6641	0.59	–	–	358	54.24
Hottah Lake	−118.484	65.0678	842.81	175	6.7	875 662	93.45
Howard Lake	−105.97	62.213	186.86	345	4	172 970	83.31
Huff Lake	−107.163	62.2876	7.96	387	4.9	6599	74.62
Hump Lake	−116.552	63.586	2.72	191	8.2	2111	69.85
Humpy Lake	−113.435	64.6678	23.77	402	8.2	23 502	88.98
Hunter Lake	−113.371	64.1024	9.9	362	8.9	9181	83.43
Indian Hill Lake	−110.736	63.222	90.09	380	4.1	82 097	82.02
Indian Mountain Lake	−111.004	63.1267	23.55	387	15.6	21 855	83.52
Indin Lake	−115.151	64.2435	156.43	253	45.2	150 631	86.66
Inglis Lake	−115.164	63.1693	16.49	201	17.2	13 740	75.02
Ingray Lake	−116.171	64.2701	139.71	241	62.9	142 207	91.6
Irritation Lake	−115.264	65.0587	4.3	382	7.1	4019	84.19
Isabella Lake	−117.697	64.8136	59.6	186	26.9	60 442	91.19
Island Lake	−114.1	62.4914	0.9	205	3.3	563	56.67
Itchen Lake	−112.827	65.5184	137.71	400	23.1	144 870	94.68
Jackfish Lake	−114.392	62.4666	0.47	182	5	376	72.34
Jackson Lake	−114.305	62.5872	0.92	182	5.2	654	64.13
James Lake	−116.439	63.0095	19.34	147	15.8	17 730	82.52
Jennejohn Lake	−113.747	62.4206	16.98	196	4.6	15 192	80.51
Jim Lake	−104.579	62.4087	20.33	282	5.7	20 581	91.1
Joe Lake	−114.387	62.483	0.1	–	–	45	40
Johnston Lake	−114.2	62.9965	5.34	213	10.6	4969	83.71
Jolly Lake	−111.94	64.1417	73.43	403	9.8	75 697	92.78
Jones Lake	−108.377	62.3131	4.53	367	7.7	3984	79.25
Kam Lake	−114.406	62.4205	2.12	163	4.7	1770	75
Kamilukuak Lake	−102.005	62.4711	0.34	247	21.1	235	61.76
Keskarrah Lake	−115.25	66.0464	18.73	399	8.3	17 792	85.37
King Lake	−110.762	63.7752	13.04	402	5.7	12 294	84.82
Kirk Lake	−109.066	63.7188	64.1	389	5.7	64 275	90.25
Kog Lake	−114.396	62.4048	0.63	170	3.3	349	49.21
Koropchuk Lake	−116.767	64.1512	27.7	241	9.4	23 818	77.4
Kway Cha Lake	−118.552	65.4413	23.96	166	2.8	23 902	89.69
Lac La Loche	−110.877	62.006	2.65	301	6.3	2423	82.26
Lac Avril	−115.292	63.9542	1.35	253	9.9	1123	74.81
Lac de Charloit	−107.976	63.8105	102.31	375	13.5	104 407	91.85

Table A1. Continued.

Lake name	Latitude (°)	Longitude (°)	Area (km^2)	Elevation (m)	Average depth (m)	Number of pixels	Percentage of lake represented
Lac du Bois	−105.76	63.6146	13.71	343	3.8	12 312	80.82
Lac Grandin	−119.064	63.9802	244.36	319	6.1	263 747	97.14
Lac la Martre	−117.961	63.3195	1676.65	249	10	1 815 957	97.34
Lac la Prise	−108.722	63.062	30.61	375	9.9	29 779	87.55
Lac Levis	−117.951	62.6347	53.25	265	3.7	56 088	94.8
Lac Malfait	−117.988	64.6284	38.05	174	4.8	38 337	90.67
Lac Nez Croche	−111.403	63.2502	28.59	396	9.7	27 563	86.78
Lac Tachs	−119.987	64.0127	124.55	308	13.5	126 349	91.3
Lac Tate d'Ours	−110.572	63.3577	62.23	385	10	63 718	92.16
Lake of the Enemy	−110.238	63.7792	135.33	396	12.2	134 187	89.06
Lake Providence	−112.065	64.7582	102.58	358	28	103 207	90.55
Lamoureux Lake	−113.682	62.9108	4.11	270	6.1	3551	77.86
Landing Lake	−114.408	62.56	1.28	202	2.6	861	60.16
Languish Lake	−112.904	62.7684	11.24	307	4.4	10 597	84.88
Larocque Lake	−107.707	63.0496	1.5	396	2.5	1108	66.67
Lastfire Lake	−113.029	64.5342	6.13	357	6.4	5919	86.95
Laurie Lake	−115.208	64.4817	0.47	358	5	330	63.83
Lausen Lake	−109.744	62.5875	7.24	186	15.3	6648	82.6
Leonforte Lake	−119.654	64.5848	10.65	392	6.1	10 916	92.21
Likely Lake	−114.311	62.6466	0.39	204	4.9	130	30.77
Little Crapeau Lake	−116.518	64.8211	123.5	275	21.4	118 280	85.98
Little Forehead Lake	−113.281	64.7824	18.2	401	20	16 804	83.08
Little Lake	−113.96	62.5467	0.14	217	2.7	92	57.14
Logie Lake	−105.759	62.1353	4.23	357	2.8	3454	73.52
Long Lake	−114.442	62.4773	1.16	196	2.1	788	61.21
Long Legs Lake	−113.773	64.7613	16.7	417	5.6	14 850	80.06
Longtom Lake	−117.834	65.1715	43.93	189	19.3	43 869	89.87
Lou Lake	−116.782	63.5682	1.82	193	13.8	1468	72.53
Love Lake	−114.759	62.995	4.43	246	5.9	3172	64.33
Lynx Lake	−106.285	62.4099	295.27	344	10.1	282 676	86.16
Mac Lake	−113.468	63.0753	5.09	312	5.3	3993	70.53
MacKay Lake	−111.012	63.9233	972.33	390	20.7	1 002 573	92.8
MacLellan Lake	−110.037	63.2324	23.2	383	13.9	20 923	81.16
MacNaughton Lake	−115.314	63.7135	0.37	296	3.7	201	48.65
Mad Lake	−112.749	62.1169	1.16	222	4.1	958	74.14
Madeline Lake	−114.081	62.5468	0.93	170	8.8	733	70.97
Magpie Lake	−108.877	62.4488	4.13	355	8.8	3700	80.63
Magrum Lake	−108.635	62.0674	4.97	373	7.1	4492	81.29
Malley Lake	−108.087	63.5601	30.34	395	7.5	25 931	76.93
Mann Lake	−112.797	62.3496	1.26	244	2.2	958	68.25
Mantic Lake	−104.457	62.3336	59.48	293	5.4	58 030	87.81
Margaret Lake	−117.128	64.507	102.43	203	32.2	101 844	89.47
Marian Lake	−116.203	62.9243	236.84	147	15.8	251 024	95.22
Martin Lake	−114.439	62.5313	3.09	197	3.2	2163	63.11
Mary Frances Lake	−106.245	63.3043	149.45	363	8	143 654	86.51
Mary Lake	−103.54	62.3855	164.8	294	20.6	170 394	92.96
Mattberry Lake	−115.891	64.1132	82.24	235	38.6	80 356	87.94
Matthews Lake	−111.245	64.0696	10.35	422	6.3	9582	83.29
Max Ward Lake	−113.708	65.4787	11.65	367	8.5	11 912	92.02
Maze Lake	−105.944	63.8946	16.16	350	2.9	12 516	69.68
Mazenod Lake	−117.014	63.7003	36.3	199	14	34 834	86.36
McCrea Lake	−112.572	63.5556	16.07	404	12	15 065	84.38
McIntosh Lake	−114.901	65.7574	3.71	436	5	3398	82.48
McKee Lake	−110.043	62.3492	2.97	353	6.1	2387	72.39
McKinlay Lake	−111.541	62.8749	26.65	365	8.1	25 518	86.19
McKinnon Lake	−108.497	62.0601	10.03	370	5.6	9324	83.65
McLellan Lake	−117.958	63.8428	9.55	–	–	9510	89.63
McPhee Lake	−113.052	63.0264	1.91	312	7.2	1323	62.3
McTavish Arm	−117.83	65.4491	189.7	175	29.6	188 745	89.55
Meander Lake	−112.149	62.5774	10.48	311	10.7	9539	81.97
Meg Lake	−114.383	62.416	0.09	–	–	45	44.44
Meridian Lake	−109.43	62.6042	37.1	201	26.3	38 923	94.42

Table A1. Continued.

Lake name	Latitude (°)	Longitude (°)	Area (km^2)	Elevation (m)	Average depth (m)	Number of pixels	Percentage of lake represented
Merl Lake	−112.655	62.4007	0.7	260	3.5	550	70
Mesa Lake	−115.147	64.8268	36.55	365	12.4	34 701	85.44
Messina Lake	−119.526	64.1837	18.27	371	7	18 633	91.79
Methane Lake	−114.174	62.4838	0.98	180	3.8	684	63.27
Michel Lake	−114.141	62.881	3.17	229	6.1	2633	74.76
Milner lake	−114.341	62.5923	0.41	212	2.3	182	39.02
Misty Lake	−109.785	63.067	9.86	321	12.9	9180	83.77
Moberly Lake	−114.315	63.0166	12.75	225	20.8	10 564	74.59
Mohawk Lake	−112.115	64.0222	20.01	438	4.6	18 774	84.46
Moise Lake	−114.136	62.3247	0.78	166	3.7	596	69.23
Moose Lake	−114.089	62.9803	1.24	253	5.7	978	70.97
Moraine Lake	−106.01	64.1074	80.99	352	5.3	75 416	83.8
Morel Lake	−113.677	65.6372	20.28	380	8	19 808	87.92
Morose Lake	−112.915	62.8252	12.01	311	6	11 015	82.51
Mosquito Lake	−103.341	62.5798	311.21	292	12.7	323 804	93.54
Mud Lake	−117.197	63.0225	11.2	–	–	9829	79.02
Munn Lake	−109.974	63.6481	70.94	391	15.9	71 057	90.01
Murdock Lake	−109.431	63.5811	51.1	423	4	44 286	78
Murphy Lake	−109.801	62.1121	8.86	299	9.4	8198	83.3
Murray Lake	−113.441	63.0154	2.56	292	3.7	2187	76.95
Musclow Lake	−106.953	63.7879	4.97	375	3.2	4259	77.06
Muskeg Lake	−103.64	62.0805	8.47	322	5.4	6939	73.67
Naga Lake	−119.21	65.2199	5.31	175	5.7	5261	89.08
Nardin Lake	−113.839	63.4931	18.14	341	11.9	15 645	77.62
Nelligan Lake	−105.784	63.3149	8.66	360	4.1	7482	77.71
Nelson Lake	−108.111	62.1925	7.77	409	3.5	5840	67.7
Newbigging Lake	−112.226	64.4419	15.36	444	8	15 039	88.15
Nieznany Lake	−105.175	62.3904	3.56	323	3.9	2966	75
Nonacho Lake	−109.317	62.0843	104.88	312	15.3	104 841	89.86
No Name Lake 01	−114.39	62.5522	0.06	–	–	14	16.67
No Name Lake 02	−108.095	64.4885	50.13	379	14.1	48 651	87.35
No Name Lake 03	−109.052	64.3012	28.16	403	4.6	28 308	90.48
No Name Lake 04	−109.297	64.3279	64.28	393	6.3	65 424	91.6
No Name Lake 05	−108.275	63.7958	20.95	389	6.2	20 814	89.4
No Name Lake 06	−112.075	63.6362	70.68	413	7.3	68 296	86.97
No Name Lake 07	−110.554	63.5828	64.99	409	8.4	59 077	81.81
No Name Lake 08	−114.046	63.3532	17.4	290	28.3	16 528	85.52
No Name Lake 09	−107.279	63.3114	77.05	362	6.1	74 521	87.05
No Name Lake 10	−106.178	63.1366	47.57	349	5.9	47 674	90.2
No Name Lake 11	−117.93	62.9845	45.5	267	3.1	46 436	91.85
No Name Lake 12	−102.796	63.0017	88.98	263	4.3	86 218	87.21
No Name Lake 13	−111.917	62.9299	40.08	390	13.8	39 749	89.25
No Name Lake 14	−102.003	62.6587	34.76	246	8.7	31 634	81.9
No Name Lake 15	−114.246	62.7732	24.89	195	21.1	20 640	74.65
No Name Lake 16	−113.936	62.5755	38.89	166	20.8	36 375	84.19
No Name Lake 17	−114.194	62.5985	36.73	152	24.4	36 116	88.48
No Name Lake 18	−107.594	62.4351	48.91	362	8.7	46 675	85.89
No Name Lake 19	−103.28	62.2774	62.81	285	8.5	60 275	86.29
No Name Lake 20	−114.47	62.6374	1.1	215	4	661	53.64
No Name Lake 21	−114.421	62.5109	1.33	201	1.6	919	62.41
No Name Lake 22	−114.231	62.4853	3.21	169	5.3	2700	75.7
No Name Lake 23	−114.177	62.4598	1.39	164	2.9	1069	69.06
No Name Lake 24	−114.628	62.428	1.26	171	2.6	891	63.49
No Name Lake 25	−114.472	62.5003	0.21	204	1.9	131	57.14
No Name Lake 26	−109.632	65.0632	208.76	427	15.1	208 919	89.95
No Name Lake 27	−110.876	64.792	109.48	430	8.2	108 844	89.48
No Name Lake 28	−115.883	63.7155	139.74	208	2	129 795	83.48
No Name Lake 29	−112.318	63.4001	106.08	397	14.5	100 296	85.1
No Name Lake 30	−102.65	62.5706	194.39	255	11.7	192 351	89.06
No Name Lake 31	−114.871	65.2597	25.88	449	5.6	25 720	89.45
No Name Lake 32	−115.923	65.0306	54.52	348	18.5	52 898	87.33
No Name Lake 33	−109.082	65.024	68.24	399	10.9	71 432	94.21

Table A1. Continued.

Lake name	Latitude (°)	Longitude (°)	Area (km^2)	Elevation (m)	Average depth (m)	Number of pixels	Percentage of lake represented
No Name Lake 34	−108.844	64.9761	36.5	380	7.7	38 642	95.29
No Name Lake 35	−109.044	64.9043	19.27	417	12.8	19 406	90.66
No Name Lake 36	−108.66	64.9469	44.71	382	6.7	45 389	91.37
No Name Lake 37	−109	64.7693	65.26	397	9.9	64 212	88.55
Noyes Lake	−105.901	62.5395	24.79	346	4.3	24 435	88.71
Octopus Lake	−114.449	62.3737	0.77	158	1.8	453	53.25
Odjick Lake	−113.917	65.516	31.55	358	28	32 155	91.73
Old Canoe Lake	−111.453	63.443	61.76	421	12.5	57 663	84.03
Olson Lake	−105.277	62.9121	7.97	337	4	7755	87.58
One Arm Lake	−114.342	62.5458	0.12	183	3	37	25
Orkney Lake	−113.182	64.1307	5.96	385	5	5583	84.23
Oro Lake	−114.333	62.6283	0.46	219	3.5	231	45.65
Ortona Lake	−119.222	64.7705	14.3	634	6.2	14 279	89.86
Outram lakes	−109.433	64.0362	48.87	367	9.2	49 430	91.04
Papanakies Lake	−110.338	63.2306	23.3	406	5.7	22 211	85.79
Parent Lake	−114.381	65.2658	50.14	376	14.6	49 992	89.73
Pate Lake	−114.206	64.4237	12.02	382	7.4	11 154	83.53
Payne Lake	−112.068	62.8293	9.74	362	12.1	8904	82.24
Peaceful Lake	−113.505	62.9932	2.46	283	4.2	2119	77.64
Pellatt Lake	−109.777	64.9606	40.31	427	15.1	38 887	86.83
Pelonquin Lake	−111.225	65.3221	21.08	493	7	21 342	91.13
Peninsula Lake	−113.364	62.5234	0.84	230	4.2	501	53.57
Perlson Lake	−111.92	63.1328	24.87	394	9.1	24 483	88.58
Phoenix Lake	−113.339	63.7636	27.15	344	13.9	24 178	80.15
Pickerel Lake	−113.488	62.4943	1.57	209	6.8	1100	63.06
Pink Lake	−113.018	62.6731	3.44	263	7.4	2883	75.29
Plant Lake	−113.557	62.5236	5.31	212	7.9	5901	84.16
Plex Lake	−110.785	63.1137	2.21	389	5.8	2036	82.81
Point Lake	−113.091	65.2602	626.84	358	28	644 500	92.47
Pollock Lake	−115.808	63.3195	4.06	198	9.3	3165	70.2
Pontoon Lake	−114.003	62.5418	3.36	195	7.2	3064	82.14
Porphyry Lake	−113.403	64.0488	3.53	345	6.9	3156	80.45
Prang Lake	−112.501	63.8773	14.34	425	7.9	13 060	81.94
Preg Lake	−114.081	62.4527	0.17	173	3.3	76	41.18
Prestige Lake	−113.645	62.9615	8.25	270	6.8	7802	85.09
Price Lake	−108.158	62.0349	8.59	375	7	8341	87.43
Ptarmigan Lake	−107.429	63.5903	82.73	352	12.7	82 480	89.71
Pud Lake	−114.383	62.4316	0.17	181	2.7	96	52.94
Rabbit Lake	−116.849	63.4668	11.96	172	12.4	12 441	93.65
Raccoon Lake	−117.692	62.87	43.93	287	1	45 951	94.15
Radford Lake	−105.576	63.3944	41.05	341	4.5	39 226	85.99
Rae Lake	−117.321	64.1656	201.35	200	28.3	198 474	88.72
Range Lake	−114.423	62.4473	0.21	188	2.9	110	47.62
Ranji Lake	−115.09	64.1015	15.29	260	29.8	15 364	90.45
Rater Lake	−114.368	62.5537	0.2	182	3.8	51	25
Rawalpindi Lake	−114.623	65.0285	88.37	415	6.7	87 345	88.96
Rebesca Lake	−116.373	64.5352	65.24	252	36.5	66 388	91.46
Recluse Lake	−114.015	66.0421	0.71	376	13.5	522	66.2
Redout Lake	−113.016	62.7403	8.38	293	7.4	7423	79.71
Redrock Lake	−114.165	65.4776	83.25	358	28	82 622	89.32
Reid Lake	−109.959	63.7626	40.8	401	8.9	39 960	88.14
Reindeer Lake	−113.583	63.8865	50.25	338	10.5	49 658	88.94
Rib Lake	−114.177	62.3445	0.58	166	4	430	67.24
River Lake	−114.091	62.5945	4.96	166	20.8	4495	81.65
Robb Lake	−116.021	65.3709	16.95	356	15.4	17 118	90.91
Robert Lake	−109.357	62.3803	3.52	331	11.8	2948	75.28
Rodrigues Lake	−115.633	64.7871	5.55	296	11.5	5399	87.57
Rolfe Lake	−111.725	63.0835	55.57	402	8.2	54 011	87.48
Rome Lake	−118.342	64.3155	22.23	402	3.3	21 396	86.64
Ross Lake	−113.26	62.6815	15.7	254	7	14 207	81.46
Roulante Lake	−113.748	64.5571	20.52	420	11.4	18 449	80.9
Roundrock Lake	−113.404	64.3891	29.74	342	23.9	29 970	90.69

Table A1. Continued.

Lake name	Latitude (°)	Longitude (°)	Area (km^2)	Elevation (m)	Average depth (m)	Number of pixels	Percentage of lake represented
Rupp Lake	−112.264	63.8287	6.37	442	4.8	5234	73.94
Russell Lake	−115.75	63.0373	177.03	147	15.8	171 240	86.93
Ryan Lake	−114.372	62.5871	1.06	220	2.6	879	74.53
Samandr Lake	−115.384	65.9782	59.36	422	10.8	59 573	90.11
Sandy Lake	−113.077	64.1536	4.18	382	6.6	3763	80.86
Sarah Lake	−117.147	63.7832	66.45	187	17.3	66 049	89.45
Savannah Lake	−108.911	64.4309	29.02	393	6.6	27 969	86.73
Savoy Lake	−115.436	64.4286	1	330	7.7	773	70
Schist lakes	−109.913	62.3707	0.95	353	5.2	422	40
Scott Lake	−113.572	62.652	2.62	246	5.6	1883	64.5
Scotty Lake	−112.989	63.4673	1.67	408	8.6	1359	73.05
Seahorse Lake	−111.229	64.3086	20.41	420	5.4	20 629	90.98
Seal Lake	−108.95	64.6326	83.6	403	13.1	79 887	86
Second Lake	−117.426	62.1259	3.27	179	5.4	3122	85.93
Self Lake	−117.274	65.2949	21.46	292	14.3	20 770	87.09
Shadow Lake	−114.35	62.5662	0.06	–	–	13	16.67
Shamrock Lake	−115.012	64.7763	17.82	367	8.9	17 503	88.38
Shaw Lake	−112.765	64.6106	4.99	392	6.2	4290	77.35
Short Point Lake	−114.224	62.7569	5.69	195	21.1	5339	84.53
Sid Lake	−103.986	62.2425	289.48	296	12	304 865	94.78
Sifton Lake	−106.36	63.7027	90.93	355	6.6	75 978	75.2
Simon Lake	−117.318	65.5421	6.98	270	11.8	6211	80.09
Singing Lake	−112.925	64.3162	13.32	370	9	12 863	86.79
Sled Lake	−106.821	62.1265	23.5	380	6.4	21 841	83.66
Sleepy Dragon Lake	−112.909	62.9194	5.21	331	5.7	4748	81.96
Slemon Lake	−116.033	63.2081	44.91	138	14.7	44 378	88.82
Small Lake	−113.826	62.5185	0.74	193	5.1	547	66.22
Smart Lake	−106.822	63.4912	112.35	356	11.3	103 542	82.88
Smoky Lake	−116.495	65.9003	2.45	369	9.8	2178	80
Snelgrove Lake	−105.615	62.3356	7.59	348	4.4	6599	78.26
Sophia Lake	−114.121	62.9357	3.64	248	7.2	2327	57.42
Sosan Lake	−111.95	63.2369	5.26	432	4.6	4140	70.91
Sparrow Lake	−113.648	62.6144	12.58	237	6.4	12 077	86.41
Spencer Lake	−112.462	63.1573	13.2	375	11.8	13 060	88.86
Sphinx Lake	−115.366	64.4645	1.56	345	5.7	1351	78.21
Spider Lake	−115.145	64.5067	16.58	341	11.5	13 690	74.31
Sproule Lake	−113.478	62.7444	1.6	274	2.4	1022	57.5
Spruce Island Lake	−110.427	62.4009	1.66	171	10.3	1419	77.11
Staple Lake	−114.033	62.729	1.27	247	3.1	822	58.27
Starfish Lake	−111.61	64.3321	21.29	403	6.3	21 575	91.22
Starvation Lake	−112.731	64.8988	37.76	400	9.1	38 344	91.39
Steel Lake	−104.593	63.7203	8.98	159	8.6	8562	85.86
Sterlet Lake	−109.496	64.7214	44.66	426	15.1	41 175	82.89
Street Lake	−105.317	63.4127	15.43	326	2.8	13 352	77.9
Sunken Lake	−110.233	62.9846	1.7	259	19.1	1460	77.06
Suse Lake	−112.966	63.1386	2.36	341	4.8	1975	75.42
Sussex Lake	−108.328	64.4388	14.31	379	22	13 522	85.05
Tanco Lake	−112.223	62.4201	4.27	272	5.7	2945	62.06
Tarantula Lake	−107.95	64.521	39.79	373	7.7	38 615	87.33
Taylor Lake	−108.664	63.7853	33.13	389	10.2	32 402	88.02
Tayonton Lake	−116.544	63.2112	23.03	150	3.6	12 081	47.2
Tent Lake	−107.957	62.4281	72.1	346	12.7	67 843	84.69
Terry Lake	−113.31	62.511	4.28	226	3.5	2570	53.97
Lake Nine	−114.043	63.4579	1.59	324	5.8	1194	67.3
Thetis Lake	−113.275	63.7214	29.11	351	9.9	28 312	87.36
Thistlethwaite Lake	−113.627	63.1591	44.27	252	22.8	42 541	86.49
Thomas Lake	−119.187	65.1207	3.81	241	3.8	3568	83.99
Thompson Lake	−113.5	62.6137	2.81	252	2.9	2381	76.16
Thonokied Lake	−109.628	64.3849	129.5	394	18.3	127 553	88.55
Timberhill Lake	−106.655	62.37	16.55	363	6.3	14 940	81.27
Toad Lake	−111.746	62.7272	5.91	362	4.8	4883	74.28
Tonggot Lake	−119.697	63.9928	18.55	312	4.3	15 529	75.36

Table A1. Continued.

Lake name	Latitude (°)	Longitude (°)	Area (km^2)	Elevation (m)	Average depth (m)	Number of pixels	Percentage of lake represented
Toopon Lake	−110.439	62.3529	1.51	176	9.1	1372	81.46
Torrie Lake	−116.926	66.2355	0.52	310	7.7	430	75
Toura Lake	−108.568	62.8338	0.79	374	5	507	58.23
Trapper lake	−114.363	62.5266	0.31	182	3.1	137	38.71
Trout Lake	−114.364	62.7997	2.82	204	10.3	2400	76.6
Truce Lake	−114.886	64.5323	28.65	343	8.4	27 814	87.36
Trumper Lake	−117.582	63.5949	4.96	–	–	4201	76.21
Tsan Lake	−112.937	64.0169	12.79	374	5.6	11 773	82.88
Tuchay Lake	−119.163	65.2513	31.72	172	11.1	31 222	88.56
Tuche Lake	−117.317	64.3356	14.78	200	15.8	14 489	88.23
Tumi Lake	−116.794	63.4535	6.07	165	7.7	5620	83.36
Tyrrell Lake	−105.498	63.1246	227.09	318	9.8	220 532	87.4
Uhlman Lake	−116.799	66.1321	9.3	314	12	8538	82.58
Upper Pensive Lake	−113.393	62.7247	3.28	246	5	2718	74.7
Upper Ross Lake	−113.153	62.7296	9.22	254	7	8451	82.54
Ursula Lake	−110.459	64.8159	22.95	453	6.7	22 803	89.41
Vaillant Lake	−114.51	66.2053	2.46	329	11.2	2230	81.71
Van Lake	−113.077	63.3649	4.48	340	11.5	3780	75.89
Vee Lake	−114.35	62.5555	0.7	178	4.4	393	50
Victory Lake	−113.077	62.6708	10.37	252	4.2	9373	81.39
Vital Lake	−114.438	62.601	1.49	194	5.3	1092	65.77
Waite Lake	−113.322	62.8342	7.62	290	3.7	5495	64.96
Wallie Lake	−113.951	63.1343	0.2	285	3.4	98	45
Walmsley Lake	−108.493	63.4197	231.36	378	25.8	233 258	90.74
Walsh Lake	−114.281	62.5829	9.17	174	9.6	8030	78.84
Webb Lake	−113.125	62.8492	3.62	314	4.6	2650	65.75
Wecho Lake	−113.812	63.9602	102.43	351	16.2	97 862	85.99
Wedge Lake	−113.69	62.8632	9.87	260	7.9	8665	79.03
White Quartz Lake	−108.383	62.6897	2.6	380	6.1	2089	72.31
Whitefish Lake	−106.802	62.6983	331.46	350	11.6	326 891	88.68
Whitewolf Lake	−113.919	64.9647	52.93	419	10.1	47 837	81.33
Willow Lake	−114.215	62.3617	0.9	162	5.5	658	65.56
Windflower Lake	−118.517	62.8653	36.65	256	3.7	38 202	93.81
Windy Lake	−109.928	64.9443	8.61	440	7.4	8000	83.62
Winter Lake	−112.943	64.4877	45.27	346	11.6	46 846	93.09
Wolverine Lake	−111.38	63.2084	23.42	396	9.7	23 074	88.68
Wonnacott Lake	−116.686	63.7158	1.62	–	–	1028	57.41
Woyna Lake	−112.985	62.4704	2.52	241	6	2226	79.37
Wylie Lake	−117.011	65.6689	15.66	322	9.4	14 391	82.69
Yamba Lake	−111.376	64.9531	305.28	403	16.7	310 925	91.66
Yanik Lake	−118.631	65.3664	8.1	230	5.2	8157	90.37
Zebulon Lake	−117.853	65.0521	56.04	184	15.4	56 562	90.85
Zigzag Lake	−113.035	62.3407	5.11	200	10.9	4239	74.76
Zinto Lake	−116.396	64.1152	52.42	242	27.9	48 637	83.5
Zipper Lake	−112.522	63.7092	3.81	426	6.5	3055	72.18
Zucker Lake	−106.799	62.9326	53.17	373	4.2	47 658	80.67

Author contributions. GA was responsible for developing the methodology, conducting the analysis, writing, and visualizing the original draft. HKP and KAS supervised, provided resources, and reviewed and edited the paper.

Competing interests. The contact author has declared that none of the authors has any competing interests.

Disclaimer. Publisher's note: Copernicus Publications remains neutral with regard to jurisdictional claims in published maps and institutional affiliations.

Acknowledgements. The authors acknowledge that this research was conducted within the Chief Drygeese Territories on the tradi-

tional land of the Yellowknives Dene First Nation. The authors are grateful to the Indigenous Peoples for allowing them the opportunity to learn and conduct fieldwork on their lands. This research has been supported by funding from the Natural Sciences and Engineering Research Council (NSERC) Canada Research Chair (CRC), the NSERC Discovery Grant (RGPIN-2020-05573), the Global Water Futures (GWF) Remotely Sensed Monitoring of Northern Lake Ice project (grant no. 353374), and the Government of Northwest Territories, Environment and Natural Resources, the Cumulative Impact Monitoring Programme (project no. CIMP-212). This research was enabled in part by support provided by Compute Ontario (https://www.computeontario.ca/, last access: 17 March 2023) and the Digital Research Alliance of Canada (https://alliancecan.ca/en, last access: 17 March 2023).

Financial support. This research has been supported by the Global Water Futures (grant no. 353374).

Review statement. This paper was edited by Achim A. Beylich and reviewed by Artyom Gusarov and one anonymous referee.

References

Attiah, G., Kheyrollah Pour, H., and Scott, K. A.: North Slave Lake Surface Temperature Retrieved from Landsat Archives from 1984 to 2021, Borealis [data set], https://doi.org/10.5683/SP3/J4GMC2, 2022.

Austin, J. A. and Colman, S. M.: Lake Superior summer water temperatures are increasing more rapidly than regional temperatures: A positive ice-albedo feedback, Geophys. Res. Lett., 34, L06604, https://doi.org/10.1029/2006GL029021, 2007.

Chander, G. and Markham, B.: Revised Landsat-5 TM Radiometrie Calibration Procedures and Postcalibration Dynamic Ranges, IEEE T. Geosci. Remote, 41, 2674–2677, https://doi.org/10.1109/TGRS.2003.818464, 2003.

Chen, Y., Zhao, C., and Ming, Y.: Potential impacts of Arctic warming on Northern Hemisphere mid-latitude aerosol optical depth, Clim. Dynam., 53, 1637–1651, https://doi.org/10.1007/s00382-019-04706-3, 2019.

Collingsworth, P. D., Bunnell, D. B., Murray, M. W., Kao, Y. C., Feiner, Z. S., Claramunt, R. M., Lofgren, B. M., Höök, T. O., and Ludsin, S. A.: Climate change as a long-term stressor for the fisheries of the Laurentian Great Lakes of North America, Rev. Fish Biol. Fish., 27, 363–391, https://doi.org/10.1007/s11160-017-9480-3, 2017.

Crosman, E. T. and Horel, J. D.: Remote Sensing of Environment MODIS-derived surface temperature of the Great Salt Lake, Remote Sens. Environ., 113, 73–81, https://doi.org/10.1016/j.rse.2008.08.013, 2009.

Desai, A. R., Austin, J. A., Bennington, V., and McKinley, G. A.: Stronger winds over a large lake in response to weakening air-to-lake temperature gradient, Nat. Geosci., 2, 855–858, https://doi.org/10.1038/ngeo693, 2009.

Eerola, K., Rontu, L., Kourzeneva, E., Pour, H. K., and Duguay, C.: Impact of partly ice-free Lake Ladoga on temperature and cloudiness in an anticyclonic winter situation – a case study using a limited area model, Tellus A, 66, 23929, https://doi.org/10.3402/tellusa.v66.23929, 2014.

Environment and Climate Change Canada, Université de Montréal: CIMP 161_Legacy arsenic pollution in Yellowknife Bay sediments, 1.0.0, DataStream [data set], https://doi.org/10.25976/gm49-2a19, 2020.

Fichot, C. G., Matsumoto, K., Holt, B., Gierach, M. M., and Tokos, K. S.: Assessing change in the overturning behavior of the Laurentian Great Lakes using remotely sensed lake surface water temperatures, Remote Sens. Environ., 235, 111427, https://doi.org/10.1016/j.rse.2019.111427, 2019.

Hersbach, H., Bell, B., Berrisford, P., Biavati, G., Horányi, A., Muñoz Sabater, J., Nicolas, J., Peubey, C., Radu, R., Rozum, I., Schepers, D., Simmons, A., Soci, C., Dee, D., and Thépaut, J.-N.: ERA5 hourly data on single levels from 1959 to present, Copernicus Climate Change Service (C3S) Climate Data Store (CDS) [data set], https://doi.org/10.24381/cds.adbb2d47, 2018.

Hersbach, H., Bell, B., Berrisford, P., Hirahara, S., Horányi, A., Muñoz-Sabater, J., Nicolas, J., Peubey, C., Radu, R., Schepers, D., Simmons, A., Soci, C., Abdalla, S., Abellan, X., Balsamo, G., Bechtold, P., Biavati, G., Bidlot, J., Bonavita, M., De Chiara, G., Dahlgren, P., Dee, D., Diamantakis, M., Dragani, R., Flemming, J., Forbes, R., Fuentes, M., Geer, A., Haimberger, L., Healy, S., Hogan, R. J., Hólm, E., Janisková, M., Keeley, S., Laloyaux, P., Lopez, P., Lupu, C., Radnoti, G., De Rosnay, P., Rozum, I., Vamborg, F., Villaume, S., and Thépaut, J.-N.: The ERA5 global reanalysis, Q. J. Roy. Meteorol. Soc., 146, 1999–2049, https://doi.org/10.1002/qj.3803, 2020.

Huang, Y., Liu, H., Hinkel, K., Yu, B., Beck, R., and Wu, J.: Analysis of Thermal Structure of Arctic Lakes at Local and Regional Scales Using in Situ and Multidate Landsat-8 Data, Water Resour. Res., 53, 9642–9658, https://doi.org/10.1002/2017WR021335, 2017.

HydroSheds: HydroLAKES, Hydrosheds [data set], https://www.hydrosheds.org/products/hydrolakes, last access: 20 May 2022.

Ihlen, V. and Zanter, K.: Landsat 7 (L7) Data Users Handbook, USGS Landsat User Serv., 7, 151, https://d9-wret.s3.us-west-2.amazonaws.com/assets/palladium/production/s3fs-public/atoms/files/LSDS-1927_L7_Data_Users_Handbook-v2.pdf (last access: 6 March 2023), 2019.

Irons, J. R., Dwyer, J. L., and Barsi, J. A.: The next Landsat satellite: The Landsat Data Continuity Mission, Remote Sens. Environ., 122, 11–21, https://doi.org/10.1016/j.rse.2011.08.026, 2012.

Jiménez-Muñoz, J. C. and Sobrino, J. A.: A generalized single-channel method for retrieving land surface temperature from remote sensing data, J. Geophys. Res, 108, 4688, https://doi.org/10.1029/2003JD003480, 2003.

Jimenez-Munoz, J. C., Cristobal, J., Sobrino, J. A., Sòria, G., Ninyerola, M., and Pons, X.: Revision of the single-channel algorithm for land surface temperature retrieval from landsat thermal-infrared data, IEEE T. Geosci. Remote, 47, 339–349, https://doi.org/10.1109/TGRS.2008.2007125, 2009.

Jimenez-Munoz, J. C., Sobrino, J. A., Skokovic, D., Mattar, C., and Cristobal, J.: Land surface temperature retrieval methods from landsat-8 thermal infrared sensor data, IEEE Geosci. Remote Sens. Lett., 11, 1840–1843, https://doi.org/10.1109/LGRS.2014.2312032, 2014.

Kheyrollah Pour, H., Duguay, C. R., Solberg, R., and Rudjord, Ø.: Impact of satellite-based lake surface observations on the ini-

tial state of HIRLAM. Part I: Evaluation of remotelysensed lake surface water temperature observations, Tellus A, 66, 21534, https://doi.org/10.3402/tellusa.v66.21534, 2014a.

Kheyrollah Pour, H., Rontu, L., Duguay, C., Eerola, K., and Kourzeneva, E.: Impact of satellite-based lake surface observations on the initial state of HIRLAM. Part II: Analysis of lake surface temperature and ice cover, Tellus A, 66, 21395, https://doi.org/10.3402/tellusa.v66.21395, 2014b.

Kheyrollah Pour, H., Duguay, C. R., Scott, K. A., and Kang, K. K.: Improvement of Lake Ice Thickness Retrieval from MODIS Satellite Data Using a Thermodynamic Model, IEEE T. Geosci. Remote, 55, 5956–5965, https://doi.org/10.1109/TGRS.2017.2718533, 2017.

Kraemer, B. M., Anneville, O., Chandra, S., Dix, M., Kuusisto, E., Livingstone, D. M., Rimmer, A., Schladow, S. G., Silow, E., Sitoki, L. M., Tamatamah, R., Vadeboncoeur, Y., and McIntyre, P. B.: Morphometry and average temperature affect lake stratification responses to climate change, Geophys. Res. Lett., 42, 4981–4988, https://doi.org/10.1002/2015GL064097, 2015.

Livingstone, D. M., Lotter, F., and Kettle, H.: Altitude-dependent differences in the primary physical response of mountain lakes to climatic forcing, Limnol. Oceanogr., 50, 1313–1325, 2005.

Magnuson, J. J., Robertson, D. M., Benson, B. J., Wynne, R. H., Livingstone, D. M., Arai, T., Assel, R. A., Barry, R. G., Card, V., Kuusisto, E., Granin, N. G., Prowse, T. D., Stewart, K. M., and Vuglinski, V. S.: Historical trends in lake and river ice cover in the Northern Hemisphere, Science, 289, 1743–1746, https://doi.org/10.1126/science.289.5485.1743, 2000.

Markham, B., Barsi, J., Kvaran, G., Ong, L., Kaita, E., Biggar, S., Czapla-Myers, J., Mishra, N., and Helder, D.: Landsat-8 operational land imager radiometric calibration and stability, Remote Sensing, 6, 12275–12308, https://doi.org/10.3390/rs61212275, 2014.

Merchant, C. J., Paul, F., Popp, T., Ablain, M., Bontemps, S., Defourny, P., Hollmann, R., Lavergne, T., Laeng, A., de Leeuw, G., Mittaz, J., Poulsen, C., Povey, A. C., Reuter, M., Sathyendranath, S., Sandven, S., Sofieva, V. F., and Wagner, W.: Uncertainty information in climate data records from Earth observation, Earth Syst. Sci. Data, 9, 511–527, https://doi.org/10.5194/essd-9-511-2017, 2017.

Messager, M. L., Lehner, B., Grill, G., Nedeva, I., and Schmitt, O.: Estimating the volume and age of water stored in global lakes using a geo-statistical approach, Nat. Commun., 7, 13603, https://doi.org/10.1038/ncomms13603, 2016.

Le Moigne, P., Colin, J., and Decharme, B.: Impact of lake surface temperatures simulated by the FLake scheme in the CNRM-CM5 climate model, Tellus A, 68, 31274, https://doi.org/10.3402/tellusa.v68.31274, 2016.

Natural Resources Canada: Lakes, Rivers and Glaciers in Canada – CanVec Series – Hydrographic Features, Government of Canada [data set], https://open.canada.ca/data/en/dataset/9d96e8c9-22fe-4ad2-b5e8-94a6991b744b (last access: 28 March 2022), 2019.

O'Reilly, C. M., Rowley, R. J., Schneider, P., Lenters, J. D., Mcintyre, P. B., and Kraemer, B. M.: Rapid and highly variable warming of lake surface waters around the globe, Geophys. Res. Lett., 42, 10773–10781, https://doi.org/10.1002/2015GL066235, 2015.

Pekel, J. F., Cottam, A., Gorelick, N., and Belward, A. S.: High-resolution mapping of global surface water and its long-term changes, Nature, 540, 418–422, https://doi.org/10.1038/nature20584, 2016.

Prats, J., Reynaud, N., Rebière, D., Peroux, T., Tormos, T., and Danis, P.-A.: LakeSST: Lake Skin Surface Temperature in French inland water bodies for 1999–2016 from Landsat archives, Earth Syst. Sci. Data, 10, 727–743, https://doi.org/10.5194/essd-10-727-2018, 2018.

Reinart, A. and Reinhold, M.: Mapping surface temperature in large lakes with MODIS data, Remote Sens. Environ., 112, 603–611, https://doi.org/10.1016/j.rse.2007.05.015, 2008.

Roy, D. P., Wulder, M. A., Loveland, T. R., C. E., W., Allen, R. G., Anderson, M. C., Helder, D., Irons, J. R., Johnson, D. M., Kennedy, R., Scambos, T. A., Schaaf, C. B., Schott, J. R., Sheng, Y., Vermote, E. F., Belward, A. S., Bindschadler, R., Cohen, W. B., Gao, F., Hipple, J. D., Hostert, P., Huntington, J., Justice, C. O., Kilic, A., Kovalskyy, V., Lee, Z. P., Lymburner, L., Masek, J. G., McCorkel, J., Shuai, Y., Trezza, R., Vogelmann, J., Wynne, R. H., and Zhu, Z.: Landsat-8: Science and product vision for terrestrial global change research, Remote Sens. Environ., 145, 154–172, https://doi.org/10.1016/j.rse.2014.02.001, 2014.

Schneider, P. and Hook, S. J.: Space observations of inland water bodies show rapid surface warming since 1985, Geophys. Res. Lett., 37, L22405, https://doi.org/10.1029/2010GL045059, 2010.

Sentlinger, G. I., Hook, S. J., and Laval, B.: Sub-pixel water temperature estimation from thermal-infrared imagery using vectorized lake features, Remote Sens. Environ., 112, 1678–1688, https://doi.org/10.1016/j.rse.2007.08.019, 2008.

Shi, Q. and Xie, P.: Impact of lake surface temperature variations on lake effect snow over the great lakes region, J. Geophys. Res.-Atmos., 124, 12553–12567, https://doi.org/10.1029/2019JD031261, 2019.

Sima, S., Ahmadalipour, A., and Tajrishy, M.: Mapping surface temperature in a hyper-saline lake and investigating the effect of temperature distribution on the lake evaporation, Remote Sens. Environ., 136, 374–385, https://doi.org/10.1016/j.rse.2013.05.014, 2013.

Slater, J. A., Garvey, G., Johnston, C., Haase, J., Heady, B., Kroenung, G., and Little, J.: The SRTM data "finishing" process and products, Photogramm. Eng. Remote Sensing, 72, 237–247, https://doi.org/10.14358/PERS.72.3.237, 2006.

Statistics Canada: 2016 Census-Boundary files, Statistics Canada [data set], https://www12.statcan.gc.ca/census-recensement/2011/geo/bound-limit/files-fichiers/ghy_000c06a_e.zip, last access: 30 March 2022.

U.S. Geological Survey: Landsat 8 Data Users Handbook, Nasa, 8, 97, 2016.

USGS: landsat-level-1-processing-details, https://www.usgs.gov/landsat-missions/landsat-level-1-processing-details, last access: 11 March 2022.

Wan, Z., Zhang, Y., Zhang, Q., and Li, Z. L.: Validation of the land-surface temperature products retrieved from terra moderate resolution imaging spectroradiometer data, Remote Sens. Environ., 83, 163–180, https://doi.org/10.1016/S0034-4257(02)00093-7, 2002.

Wang, J., Xue, P., Pringle, W., Yang, Z., and Qian, Y.: Impacts of lake surface temperature on the summer climate over the Great

Lakes Region, J. Geophys. Res.-Atmos., 127, e2021JD036231, https://doi.org/10.1029/2021JD036231, 2022.

Wloczyk, C., Richter, R., Borg, E., and Neubert, W.: Sea and lake surface temperature retrieval from Landsat thermal data in Northern Germany, Journal of Remote Sensing, 27, 2489–2502, https://doi.org/10.1080/01431160500300206, 2006.

Woolway, R. I., Merchant, C. J., Van Den Hoek, J., Azorin-Molina, C., Nõges, P., Laas, A., Mackay, E. B., and Jones, I. D.: Northern Hemisphere Atmospheric Stilling Accelerates Lake Thermal Responses to a Warming World, Geophys. Res. Lett., 46, 11983–11992, https://doi.org/10.1029/2019GL082752, 2019.

Woolway, R. I., Kraemer, B. M., Lenters, J. D., Merchant, C. J., O'Reilly, C. M., and Sharma, S.: Global lake responses to climate change, Nat. Rev. Earth Environ., 1, 388–403, https://doi.org/10.1038/s43017-020-0067-5, 2020.

Xie, C., Zhang, X., Zhuang, L., Zhu, R., and Guo, J.: Analysis of surface temperature variation of lakes in China using MODIS land surface temperature data, Scientific Reports, 12, 2415, https://doi.org/10.1038/s41598-022-06363-9, 2022.

Yang, K., Yu, Z., and Luo, Y.: Analysis on driving factors of lake surface water temperature for major lakes in Yunnan-Guizhou Plateau, Water Res., 184, 116018, https://doi.org/10.1016/j.watres.2020.116018, 2020.

Young, N. E., Anderson, R. S., Chignell, S. M., Vorster, A. G., Lawrence, R., and Evangelista, P. H.: A survival guide to Landsat preprocessing, Ecology, 98, 920–932, https://doi.org/10.1002/ecy.1730, 2017.

Zhang, G., Yao, T., Chen, W., Zheng, G., Shum, C. K., Yang, K., Piao, S., Sheng, Y., Yi, S., Li, J., O'Reilly, C. M., Qi, S., Shen, S. S. P., Zhang, H., and Jia, Y.: Regional differences of lake evolution across China during 1960s–2015 and its natural and anthropogenic causes, Remote Sens. Environ., 221, 386–404, https://doi.org/10.1016/j.rse.2018.11.038, 2019.

Zhang, X., Duan, K. Q., Shi, P. H., and Yang, J. H.: Effect of lake surface temperature on the summer precipitation over the Tibetan Plateau, J. Mt. Sci., 13, 802–810, https://doi.org/10.1007/s11629-015-3743-z, 2016.

Zhao, G., Gao, H., and Cai, X.: Estimating lake temperature profile and evaporation losses by leveraging MODIS LST data, Remote Sens. Environ., 251, 112104, https://doi.org/10.1016/j.rse.2020.112104, 2020.